Deep Impurity States in Molecular Clusters. Site-Specific Electronic Spectroscopy of Surface and Interior States in $XeAr_N$ Clusters

Alexander Goldberg, Andreas Heidenreich,† and Joshua Jortner*

School of Chemistry, Tel-Aviv University, Ramat Aviv, 69978 Tel Aviv, Israel

Received: September 26, 1994[⊗]

In this paper we utilize the molecular dynamics spectral density method to explore the absorption line shapes of the $^1S_0 \rightarrow {}^3P_1(6s[3/2]_1)$ electronic excitation of Xe in $XeAr_N$ ($N = 12-206$) over the temperature range $T = 10-40$ K, with the Xe atom being located in distinct substitutional sites of the heterocluster (at $T \leq 30$ K), or in an interior position in nonrigid and in amorphous clusters. The $Xe(^1S_0 \rightarrow {}^3P_1)$ extravalence excitations provide a sensitive microscopic probe for the local microenvironment of the Xe atom in these elemental clusters. The electronic excitations of Xe were described by the modified tight binding scheme (Webber, S.; Jortner, J.; Rice, S. A. *J. Chem. Phys.* **1965**, *42*, 1907) with reliable $Xe(^3P_1)-Ar(^1S_0)$ excited-state exp-6 pair potentials (Messing, I.; Raz, B.; Jortner, J. *J. Chem. Phys.* **1977**, *66*, 2239). The site-specific and cluster-size-dependent spectroscopic observables were characterized in terms of the blue spectral shift $\delta\nu$ of the absorption band peak, the spectral line width (FWHM) Γ of the band, the spectral line shape, and their temperature dependence. The simulated spectra reveal an atomic shell structure with a hierarchy of Xe occupied site-specific spectral shifts decreasing in the order $\delta\nu$(central site) > $\delta\nu$(interior sites) > $\delta\nu$(substitutional surface sites) > $\delta\nu$(top atom), providing a spectroscopic method for the interrogation of the site-specific local structure. A quantification of the site specificity and the temperature dependence of $\delta\nu$ was obtained in terms of its (nearly size invariant) exponential dependence on the average Xe−Ar nearest-neighbor distance, with the preexponential being proportional to the number of the nearest neighbors. We provided a spectroscopic identification of three temperature induced configurational changes in $XeAr_N$ clusters, i.e., a center ⇄ surface dynamic isomerization of Xe in $XeAr_{12}$ at $T > 30$ K, cluster configurational dilation around the central Xe atom in $XeAr_N$ ($N \geq 54$ with $T \geq 13$ K for $N = 54$ and 35 K < T < 40 K for $N = 146$), and surface melting. The confrontation between the theory and experimental spectroscopic data (Möller, T. *Z. Phys. D* **1991**, *20*, 1. Lengen, M.; Joppien, M.; Müller, R.; Wörmer, J.; Möller, T. *Phys. Rev. Lett.* **1992**, *68*, 2362) for large $XeAr_N$ ($N > 130$) clusters allowed for the identification of the Xe-occupied site-specific excitations of the central, interior and substitutional surface sites, while no evidence was obtained for the existence of the top atom site, which is precluded by surface melting. From the simulated temperature dependence of $\delta\nu$ for the central site in large ($N = 146-200$) clusters, the cluster temperature was estimated to be $T = 30-35$ K. For $XeAr_{12}$ we were able to identify the excitations of the center and surface sites at $T = 30$ K. Finally, the effects of nuclear dynamics on the spectra were inferred from the analysis of the power spectra of the energy gap correlation function, which established the dominance of the stochastic slow modulation limit for the line broadening.

I. Prologue

The notion of packing of particles into clusters can be traced to the early attempts to build a scientific basis for chemistry. Robert Boyle in his book *The Sceptical Chymist*, published in 1661, considered "minute clusters...as were not easily dissipable into such particles as composed them". About 300 years later the genesis of the conceptual framework for modern cluster chemical physics originated from structural considerations for close packing of hard spheres[1,2] and from the exploration of van der Waals molecules containing rare-gas atoms.[3] In an unpublished work in November 1962, which was inspired by the discovery of the rare-gas halides,[4] Rice, Jortner, and Cohen proposed the existence of a $Xe{\cdot}F_2$ cluster of triangular structure, which is stabilized by charge-transfer interactions[5] between the Xe atom and the F_2 molecule. This weakly bound $Xe{\cdot}F_2$ cluster was not experimentally observed at that time. Only 15 years later, such a weakly bound rare-gas atom−halogen molecule van der Waals cluster, i.e., $He{\cdot}I_2$, was discovered by Smalley, Levy, and Wharton,[6] opening new avenues for the exploration of the energetics, spectroscopy and dynamics of clusters.

A key concept for the quantification of the novel and unique characteristics of atomic and molecular clusters[7-24] pertains to size effects. These involve the evolution of structural, thermodynamic, electronic, energetic, electromagnetic, dynamic, and chemical features of finite systems with increasing the cluster size. Cluster size effects fall into two distinct domains:[24]

(I) Specific size effects. In the "small cluster" size domain an irregular size dependence of the relevant cluster properties $\chi(n)$ (where n is the number of constituents) is exhibited. This irregular pattern is manifested most dramatically in the existence of "magic numbers" in $\chi(n)$ vs n, which reflects shell closure effects. Typical examples involve the structural closed shells of Mackay icosahedra in clusters of rare-gas atoms[1,2,25-28] and of spherical large molecules,[29] the enhanced energetic stability and increased ionization potentials for electronic closed shells in metal clusters,[30] and the expected increased stability of the Fermion closed shell structure in $(^3He)_N$ clusters.[31-33]

† Present Address: Arbeitsgruppe Quantenchemie an der Humboldt-Universität, Max-Planck-Gesellschaft, Jägerstrasse 10/11, 10117 Berlin, Germany.

[⊗] Abstract published in *Advance ACS Abstracts,* February 1, 1995.

0022-3654/95/2099-2662$09.00/0 © 1995 American Chemical Society

(II) Smooth size effects, which are revealed for "large" clusters. In this size domain a unified, but not universal, description was advanced[24] for the merging between the properties of microscopic large finite systems and those of the macroscopic bulk material in terms of cluster size equations (CSEs), $\chi(n) = \chi(\infty) + An^{-\beta}$, where A is the constant and β ($\beta \geq 0$) is a positive exponent. The CSEs specify the "critical" cluster size for which a specific property becomes size invariant and does not differ in any significant way from that of a macroscopic sample of that material.

Linear optical electronic spectroscopy of $M{\cdot}A_N$ clusters, consisting of a guest atom or molecule (M) embedded in an atomic cluster of rare-gas atoms (A), allows for the exploration of both specific and smooth structural, energetic and dynamic cluster size effects.[34-60] Spectroscopic studies of excited-state energetics, and homogeneous and inhomogeneous line broadening of heteroclusters pertain to the elucidation of microscopic solvation, isomer structures, surface and interior impurity states, rigid and nonrigid configurations, isomerization dynamics, reactive dynamics, and the evolution of bulk condensed matter and macrosurface properties with increasing the cluster size.[34-60] A wealth of information has accumulated regarding intravalence electronic excitations of $M{\cdot}A_N$ heteroclusters, where M is an aromatic organic molecule.[34-57] Extravalence electronic excitations of rare-gas heteroclusters, i.e., $XeAr_N$[57-60] are of considerable interest for the elucidation of spectra−structure relationships in elemental heteroclusters. Möller and his colleagues have obtained extensive and significant experimental data on the spectroscopy of $XeAr_N$ clusters.[57-60] The energetics of the lowest extravalence excitations of Xe in $XeAr_N$ is expected to be extremely sensitive to the local environment, providing ways and means for the exploration of the microscopic environment of the Xe atom in these elemental clusters. Pertinent information on local medium perturbations on electronic excitations of Xe in Ar clusters can be inferred from the spectroscopy of rare-gas atoms in bulk solid,[61-65] liquid,[61,66,67] and fluid[61,68-70] rare gases. A universal feature of such extravalence Xe impurity excitations $^1S_0 \rightarrow {}^3P_1$ ($^2P_{3/2}6s[3/2]_1$) and $^1S_0 \rightarrow {}^1P_1$ ($^2P_{1/2}6s'[1/2]_1$) in insulators involves a large blue spectral shift (relative to the isolated atom), which is density, structure and temperature dependent.[61-70] The modified tight binding scheme advanced by Webber, Rice, and Jortner[71] considers the lowest extravalence electronic excitation(s) of an impurity atom in an insulator to have a unique parentage in the extravalence excitation(s) of the isolated atom. This approach differs from the alternative modified Wannier scheme,[61,72] which considers an $n = 1$ Wannier excitation subjected to large central cell corrections, which is of some use for solids.[72] Within the modified tight binding scheme the spectral shift originates from a delicate balance between repulsive nonorthogonality overlap-exchange interactions, which result in large positive energy corrections, and between dispersive and charge-transfer interactions, which contribute to negative energy corrections. The former short-range repulsive contribution dominates the energy shift, resulting in an appreciable blue spectral shift, in general accord with experiment.[61-70] The tight binding scheme can be modelled into excited-state pair potentials.[68,69] Excited-state pair potentials for $Xe(^3P_1)-Ar(^1S_0)$ and $Xe(^1P_1)-Ar(^1S_0)$ were derived by Messing, Raz, and Jortner[68,69] from a fit of the absorption spectra of Xe in fluid Ar over a broad density range from the low-pressure gas phase up to the liquid. These reliable potential parameters provide central information for the simulations of the optical spectra of $XeAr_N$ clusters.

In this paper we apply the semiclassical spectral density method[73] for the molecular dynamics (MD) simulations of the line shapes of the lowest one-photon allowed $Xe(^1S_0 \rightarrow {}^3P_1)$ electronic excitation in $XeAr_N$ ($N = 12-206$) clusters. The optical line-shape simulations, in conjunction with the available experimental data,[57-60] pertain to the following information:

(1) The distinction between interior and surface configuration of the impurity guest atom in and on the elemental cluster. Until now infrared[74] and photoelectron[75-78] spectroscopy of molecular and ionic clusters provided a coarsed-grained distinction between interior and surface states of the guest. The electronic spectroscopy of $XeAr_N$ will allow for a detailed interrogation of the location of the Xe impurity in and on the cluster.

(2) Identification of distinct surface configurations. These involve different substitutional sites of the Xe on the surface as well as the absorption of the Xe atom on the top of the cluster surface. These distinct surface sites will be specified by different spectral shifts.

(3) Spectroscopic probing of the atomic shell structure in the rare-gas clusters. Until now the pertinent information emerged only from structural data.[1,2,25-28] Different spectral shifts will be exhibited for distinct interior configurations of the impurity atom, providing a new approach for probing the structure of heteroclusters.

(4) Probing of temperature-induced cluster structural changes, i.e., local configurational changes around the impurity, surface melting[79] and global cluster rigid−nonrigid transitions.[80-85]

(5) Interrogating the role of local, e.g., surface and global structural disorder on spectra, i.e., studies of the spectroscopy of liquid and amorphous clusters.

(6) Quantifying the energetics of the blue spectral shifts and the structure−spectra relationship for extravalence excitations.

(7) Determining the first and second moments of the spectral lines and their temperature dependence.

(8) Distinguishing between homogeneous and inhomogeneous line broadening.

(9) Investigating the effects of nuclear dynamics on homogeneous line broadening, which provides a microscopic description of the nature of (slow and fast) medium modulation, which determines the shape and width of the spectral lines.

We shall explore structure−spectra relationships, which emerge from spectroscopic and dynamic information for extravalence excitations of $XeAr_N$ clusters.

II. Simulations

A. Molecular Dynamics. We performed classical constant energy MD simulations as previously described.[86-88] The thermal equilibration procedure of an initial structure at a temperature T was carried out by the iterative rescaling of the velocities. Subsequently, constant energy trajectories were generated in the ground electronic state for 0.5−1.0 ns. Typical integration time steps were 0.5−10 fs. Energy conservation was better than 1 part in 10^6.

$XeAr_N$ clusters in the ground electronic state were prepared in the size domain $N = 12-206$ over the temperature range $T = 5-50$ K. Rigid structures were realized for $T < 40$ K (the upper limit for the temperature depending on N). The initial structures were characterized by using a conjugate gradient quenching technique[89] to find the stable minima on the potential surface, which underlies the classical trajectory. Doped Mackay $XeAr_N$ icosahedra ($N = 12$, 54, and 146) were prepared (at $T = 10-30$ K for $N = 12$, $T = 10-35$ K for $N = 54$, and $T = 10-40$ K for $N = 146$) with the Xe atom being substituted into each of the inequivalent sites. Structural and energetic data for the $XeAr_N$ icosahedra are displayed in Table 1. Other clusters ($N = 12-206$ at $T = 5-30$ K) were prepared by removing Ar atoms from the outer shell of the Mackay icosahedra. After equilibration the "small" ($N < 120$) clusters rearranged into other low-energy structures, the rearrangement being cluster size and temperature dependent. Proceeding now to positionally disor-

TABLE 1: Structure and Energetics of the Quenched Ar_{N+1} and $XeAr_N$ Clusters

type of cluster and substitution site for Xe[a]	equivalent sites for Xe	NN	E_{min}[b] (eV)	R_{CM} (Å)
Ar_{13}			−0.458	
$XeAr_{12}$ (central)	1	12	−0.459	0.00
$XeAr_{12}$ (surface)	12	6	−0.493	3.984
Ar_{55}			−2.883	
$XeAr_{54}$ (central)	1	12	−2.840	0.00
$XeAr_{54}$ (inner edge)	12	12	−2.924	3.507
$XeAr_{54}$ (outer edge)	30	8	−2.935	6.129
$XeAr_{54}$ (vertex)	12	6	−2.922	7.151
Ar_{147}			−9.048	
$XeAr_{146}$ (central)	1	12	−8.959	0.00
$XeAr_{146}$ (1)	12	12	−9.069	3.541
$XeAr_{146}$ (2)	12	12	−9.106	6.129
$XeAr_{146}$ (3)	12	12	−9.096	7.151
$XeAr_{146}$ (4)	20	9	−9.109	8.751
$XeAr_{146}$ (5)	60	8	−9.101	9.500
$XeAr_{146}$ (6)	12	6	−9.087	10.862

[a] Labeling of atomic spheres according to Mackay.[1] Each atomic sphere contains three inequivalent sites, i.e., the inner edge (I), the outer edge (O), and the vertex (V). The $XeAr_{54}$ and $XeAr_{146}$ clusters contain one and two atomic spheres, respectively. For $N = 146$ sites (1), (2), and (3) correspond to sites (I), (O), and (V) in the inner sphere, while sites (4), (5), and (6) correspond to sites (I), (O), and (V) in the outer sphere. [b] Ground-state cluster energy.

dered heteroclusters we studied "liquid" nonrigid $N = 54$ and $N = 146$ clusters at $T = 45-50$ K. The Xe atom resides in the interior region (for $N = 54$) of the "liquid" cluster, in accord with previous simulations.[90] Amorphous $XeAr_{146}$ clusters were prepared by equilibration at $T = 50$ K (when the Xe atom is located at the cluster center) and subsequently quenched to $T = 25$ K.

The following structural parameters are useful for the structure−spectra relations: (a) R_{CM}: The distance between the Xe atom and the center of mass of the cluster. (b) NN: The average number of Ar atoms in the nearest neighbor position to Xe. We have used the criterion[90] that any Ar atom with the Xe−Ar distance of $\leq 1.1r_e$ (where $r_e = 2^{1/6}\sigma_{Xe-Ar}$ is the equilibrium Xe−Ar separation) counts as a nearest-neighbor atom. (c) R_{NN}: The average distance between Xe and the first coordination shell of the Ar atoms, i.e.

$$R_{NN}(t) = [1/NN(t)] \sum_{j=1}^{NN(t)} |\vec{R}_j(t) - \vec{R}_{Xe}(t)|$$

where $NN(t)$ is the temporal nearest neighbor, $\vec{R}_{Xe}(t)$ and $\vec{R}_j(t)$ are the position vectors of the Xe atom and of a nearest-neighbor Ar, respectively.

Ensemble average observables and spectral line shapes were simulated by averaging over 20−30 trajectories in the ground electronic state of $XeAr_N$ clusters. The important issue pertains to the choice of the initial conditions. After equilibration one trajectory of 600 ps at the desired temperature was run. From this trajectory 20−30 initial points in a configurational space were sampled, ensuring the statistical independence of the sampled points.

III. Simulations of Absorption Line Shapes

MD and Monte-Carlo simulations of the optical spectra rest on two approaches: (i) The evaluation of the classical first and second spectral moments of the absorption line shape.[43,44,86,91] This approach provides a rather complete description of the spectral shifts and of the second moment of the absorption line shape. (ii) The semiclassical spectral density method.[73,86−88,92−105] This method allows for the calculation of the total line shape within the framework of some plausible approximations, i.e., retaining only second-order terms in the cumulant expansion of the generating function.

The electronic absorption line shape $L(E)$ at the photon energy E is expressed as the Fourier transform of the transition dipole autocorrelation function, $I(\tau)$, in the form[92−103]

$$L(E) = (1/\pi)Re\int_0^\infty d\tau \exp[-i(E - \omega_{eg})\tau]I(\tau) \quad (3.1)$$

where

$$I(\tau) = \langle \exp(iH_e t) \exp(-iH_g t)\rangle \quad (3.2)$$

where H_g and H_e are the ground-state and the excited-state Hamiltonians, respectively, and ω_{eg} is the 0−0 electronic energy gap of the bare Xe atom. The autocorrelation function is approximated by the spectral density method, which requires the calculation of the time-dependent energy gap:

$$U(t) = V_e(t) - V_g(t) \quad (3.3)$$

where $V_g(t)$ and $V_e(t)$ are the ground- and the excited-state potential energies, respectively. The first and second moments of the energy gap are

$$M_1 = \langle U(t)\rangle \quad (3.4)$$

$$M_2 = \langle U(t)^2\rangle \quad (3.5)$$

The central second moment of the energy gap is

$$\Delta^2 = M_2 - M_1^2 \quad (3.6)$$

Δ^2 is the total dispersion of the absorption band. The classical expressions for the first and the second moments of the absorption line shape are identical to the corresponding quantum results. The classical energy gap autocorrelation function is

$$J(\tau) = \langle U'(0)\, U'(\tau)\rangle \quad (3.7)$$

where

$$U'(\tau) = U(\tau) - \langle U\rangle \quad (3.8)$$

The Fourier transform $J(\omega)$ of $J(t)$ is obtained by the Wiener−Khintchine theorem by $J(\omega) = |U(\omega)|^2$. As a consequence of the fluctuation−dissipation theorem, the semiclassical energy correlation function $J_{SC}(\omega)$ in the frequency space is[102,103]

$$J_{SC}(\omega) = [1 + \tanh(\hbar\omega/2k_B T)]J(\omega) \quad (3.9)$$

The semiclassical absorption line shape, eq 3.1, is approximated by[102,103]

$$L(E) = (1/\pi)Re\int_0^\infty d\tau \exp[i(E - \omega_{eg} - \langle U\rangle)\tau] \exp[-g(\tau)] \quad (3.10)$$

where the correlation function is $\exp[-g(\tau)]$, and $g(\tau)$ is the two-time integral of the semiclassical energy gap autocorrelation function, eq 3.9, in the time domain, i.e.

$$g(\tau) = \int_0^\tau d\tau_1 \int_0^{\tau_1} d\tau_2\, J_{SC}(\tau_2) \quad (3.11)$$

The line shape, eq 3.10, corresponds to a microcanonical subspectrum. The averaged semiclassical absorption line shape $\bar{L}(E)$ is given by

$$\bar{L}(E) = (1/\pi)\mathrm{Re}\int_{\bar{\Omega}} dp\, dq\, \varrho(p,q)\int_0^\infty d\tau \exp[i(E - \omega_{eg} - \langle U\rangle)\tau] \exp(-g(\tau,p,q)) \quad (3.12)$$

where $q \equiv \{\vec{q}_A(0)\}$ and $p \equiv \{\vec{p}_A(0)\}$, and $\vec{q}_A(t)$ and $\vec{p}_A(t)$ are the coordinates and momenta of the atoms, A, respectively. $\varrho(p,q)$ is the distribution function of the ground electronic state in the accessible region ($\bar{\Omega}$) of the phase space. The averaging over the accessible region of the phase space was conducted by ensemble averaging over 20−30 microcanonical spectra.

IV. Spectral Moments

We have used the semiclassical method, eq 3.12, to generate the absorption spectra of $XeAr_N$ clusters. In addition, we have calculated the first and the second moments, eqs 3.4−3.6 of the line shapes. A detailed analysis of the power spectra $J(\omega)$ for $XeAr_N$ clusters (section XII) reveals that these systems correspond to the Kubo slow modulation limit.[105] In this limit the line shape is a Gaussian with the spectral shift $\delta\nu$ (relative to the bare atom) being given by the first moment M_1, i.e.

$$\delta\nu = M_1 \tag{4.1}$$

The spectral line width (FWHM) Γ is then related to the second moment M_2 by

$$\Gamma = 2.355(M_2 - M_1^2)^{1/2} \tag{4.2}$$

Indeed, all the spectral line shapes simulated by us were found to be Gaussian with the line widths being well (within <5% accuracy) described in terms of eq 4.2, thus corresponding to the Kubo slow modulation limit. Accordingly, the spectroscopic information can be well characterized by the two observables $\delta\nu$ and Γ.

We consider first the temperature dependence of $\delta\nu$ and Γ for a cluster which does not undergo thermally induced configurational changes, e.g., pushing out of the Xe atom from the center to the surface for small clusters or configurational dilation around a central Xe atom in medium-sized (N = 54, 146) clusters. In the temperature domain below the onset of configurational changes the temperature dependence of $\delta\nu$ originates from thermal expansion effects on the mean density and on the radial distribution function of the cluster,[104] resulting in a linear temperature dependence[43,86−88,104]

$$\delta\nu = A + BT \tag{4.3}$$

where A and B are constants and $A \gg BT$. The major contribution to the temperature dependence of Γ originates from (uncorrelated) short-range density fluctuations resulting in the strong temperature dependence

$$\Gamma = CT^{1/2} \tag{4.4}$$

where C is a numerical constant. Relations 4.3 and 4.4 are expected to hold for sufficiently large clusters, where the coarse-grained description of the spectroscopic observables applies.[104] For small (e.g., N = 12) clusters, a microscopic description transcending the continuum description is necessary. The temperature dependence of $\delta\nu$ and Γ provides a microscopic probe for temperature induced cluster isomerization. The deviations of $\delta\nu$ and Γ from a smooth temperature dependence for small clusters and their deviation from relations 4.3 and 4.4 for large clusters marks onsets of cluster configurational changes.

V. Potential Parameters

The present simulations are intended to provide a semiquantitative account for the structure−spectra relationships of $XeAr_N$ clusters. Accordingly, the choice of reliable potentials and, in particular, of excited-state potentials is crucial. Adopting the "art of the possible", pair potentials were used both for the ground and for the excited states. The ground-state Ar−Ar and Xe−Ar pair interactions were modeled by Lennard-Jones (LJ) pair potentials:[106]

$$V_{ij}(r) = 4\epsilon_{ij}[(\sigma_{ij}/r)^{12} - (\sigma_{ij}/r)^6] \tag{5.1}$$

where σ_{Ar-Ar} = 3.405 Å, ϵ_{Ar-Ar} = 0.0103 eV, σ_{Xe-Ar} = 3.65 Å, and ϵ_{Xe-Ar} = 0.0153 eV. Alternatively, several recent Ar−Ar ground-state potentials[107−111] were used. The excited state $Xe^*(^3P_1)$−Ar pair potential was adopted from the work of Messing, Raz, and Jortner[68] in the form of an exp-6 potential:

$$V_{Xe^*-Ar}(r) = \epsilon(1 - 6/\alpha)\{(6/\alpha)\exp[\alpha(1 - r/r_e)] - (r_e/r)^6\} \tag{5.2}$$

with the parameters[68] ϵ = 0.008 eV, r_e = 4.65 Å, and α = 15. This excited-state potential, eq 5.2, was obtained by Messing, Raz, and Jortner[68] from a detailed and satisfactory fit of the first and second moments of the spectra of Xe in fluid Ar over a broad density and temperature range from the low-pressure gas phase up to the liquid. Messing, Raz, and Jortner[68] have also examined a LJ excited state potential, eq 5.1, with the parameters σ_{Xe^*-Ar} = 4.13 Å and ϵ_{Xe^*-Ar} = 0.008 eV, which was used by Scharf, Jortner, and Landman[112] in MD simulations of Xe^*Ar_N and $Xe_2^*Ar_N$ clusters. The excited state exp-6 potential was found to be superior to a LJ potential in accounting for the density and temperature dependence of the spectra of Xe in fluid Ar.[68,69]

TABLE 2: Simulations of $\delta\nu$ and Δ for a Central Xe Atom in $XeAr_N$ Clusters (T = 10 K) Using Different $Xe^*(^3P_1)$−Ar Pair Potentials (Ground-State Potentials Are Taken in the LJ Form)

	LJ excited state		exp-6 excited state	
N	$\delta\nu$ (eV)	Γ (eV)	$\delta\nu$ (eV)	Γ (eV)
12	0.24	0.078	0.32	0.12
54	0.55	0.064	0.72	0.083
146	0.70	0.059	0.92	0.085

We assessed the sensitivity of the simulated spectroscopic observables of a central Xe atom in $XeAr_N$ (N = 12, 54, and 146) clusters on the form of the excited state $Xe^*(^3P_1)$−Ar potential (Table 2). The blue spectral shifts and the line widths calculated with the exp-6 potential are systematically higher by about 30% than those obtained with the LJ potential. The spectral shifts calculated for the excitation of a central atom in large $XeAr_N$ (N = 146) clusters at the experimental temperature $T \simeq 25-35$ K (see section XI) are in good agreement with the simulated result using the exp-6 but not the LJ excited state potential, thus demonstrating the superiority of the exp-6 potential. We have also tested the dependence of the calculated spectroscopic observables on the form of the ground-state Ar−Ar pair potential.[107−111] The $\delta\nu$ and Γ data are obtained for a central Xe atom in $XeAr_N$ (T = 10 K), using different Ar−Ar potentials, while the exp-6 potential was taken for $Xe^*(^3P_1)$−Ar in all cases. The largest deviation between different results for a fixed N is exhibited for small clusters, i.e., N = 45, where the Boyes potential[108] yields a value of $\delta\nu$, which is about 30% higher than the LJ result. The results for $\delta\nu$ and Γ for all the other potentials fall in the range ±10% around the LJ result. There is little point at present to attempt to modify the Ar−Ar potential. In what follows we shall use the ground-state LJ potentials, eq 5.1, and the exp-6 excited-state potential, eq 5.2.

VI. $XeAr_N$ (N = 12, 54, 146) Icosahedra

The substituted Mackay icosahedra constitute the energetically stable heteroclusters, as is the case for the neat clusters. The

TABLE 3: Simulations of $\delta\nu$ and Δ for a Central Atom in $XeAr_N$ Clusters (T = 10 K) Using Different Ar−Ar Potentials (exp-6 Potential Used for the $Xe^*(^3P_1)$−Ar Interactions)

	a		*b*		*c*		*d*		*e*		*f*	
N	$\delta\nu$ (eV)	Γ (eV)	$\delta\nu$ (eV)	Γ (eV)	$\delta\nu$ (eV)	Γ (eV)	$\delta\nu$ (eV)	Δ (eV)	$\delta\nu$ (eV)	Δ (eV)	$\delta\nu$ (eV)	Δ (eV)
18	0.30	0.059	0.30	0.053	0.30	0.051						
24			0.31	0.049			0.24	0.057	0.20	0.049	0.30	0.051
42	0.35	0.077	0.35	0.047	0.45	0.054	0.37	0.073	0.36	0.070	0.31	0.058
54	0.72	0.083	0.67	0.067			0.68	0.066				
146	0.92	0.085					0.86	0.064	1.036	0.069	0.72	0.064

[a] Equation 5.1. [b] Reference 107. [c] Reference 108. [d] Reference 109. [e] Reference 110. [f] Reference 111.

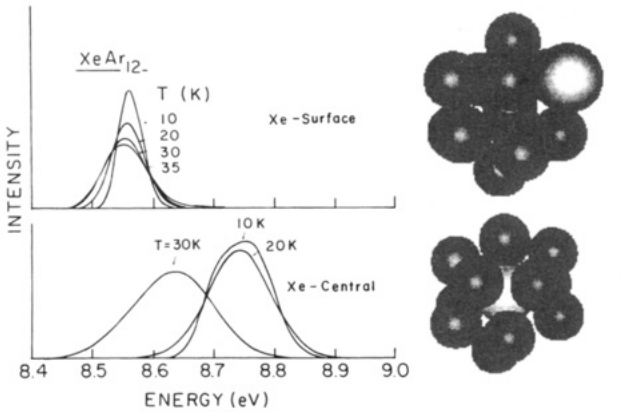

Figure 1. Temperature dependence of the line shapes of $XeAr_{12}$ clusters for (C) and (S) Xe atom substitutional sites. Snapshots of the structures are also presented.

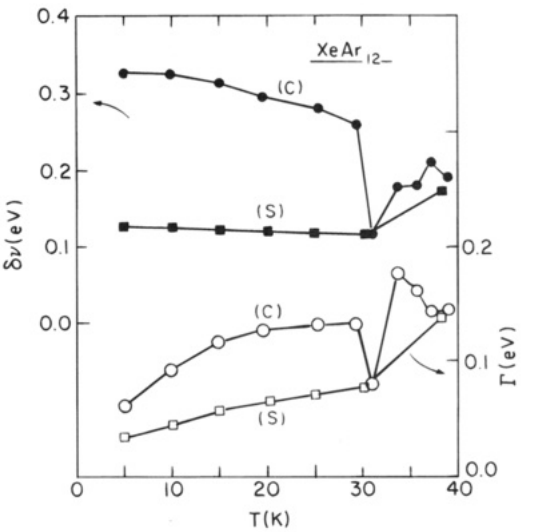

Figure 2. Temperature dependence of the spectral shift ($\delta\nu$) and the line width (Γ) for the initial (C) and (S) configurations of Xe in $XeAr_{12}$. The regular behavior of $\delta\nu$ and Γ in the range T = 5−30 K reflects structure preservation, while the irregular behavior for T > 30 K represents C ⇄ S dynamic isomerization.

study of these heteroclusters will be useful for the understanding of specific dynamic effects in smaller clusters (N = 12, 54) and nuclear shell effects in a larger (N = 146) cluster.

Simulations of ground structure and of spectra of $XeAr_{12}$ were performed both for the central configuration (the (C) site) and for the surface configuration (the (S) site) of the Xe atom (Figure 1). The structure of $XeAr_{12}$ (Figure 1), with the Xe atom in the center, preserves the configuration with NN = 12 up to T = 30 K. At T > 30 K the ground-state nuclear configuration of the initially central Xe is changed, as manifested by a drastic reduction in the NN, with the average number of nearest neighbors to Xe decreasing from NN = 10.8 at T = 30 K to NN = 5.3 at T = 31 K and NN = 7.8 at T = 35 K, indicating that the central Xe atom is pushed out and subsequently moves back and forth between the (C) site and the (S) site. The spectra (Figure 1) are "normal" up to T = 30 K, with the spectral shifts (Figure 2) weakly decreasing with increasing T. The temperature dependence of $\delta\nu$ is in accord with the linear relation, eq 4.3. The line widths (Figure 2) increase with increasing T. The cluster size is too small to warrant the applicability of eq 4.4. We note that the temperature dependence of $\delta\nu$ and of Γ, both for the central and surface Xe atom configurations, change smoothly with increasing the temperature up to $T \leq$ 30 K. Above T > 30 K the behavior of $\delta\nu$ and Γ is erratic, with the data for the initial central Xe converging to those of the initial surface Xe configuration. From the electronic spectroscopy of $XeAr_{12}$ with the Xe atom in the (C) and (S) sites we infer the following: (1) The largest spectral shift is for the (C) site, i.e., $\delta\nu$(C) > $\delta\nu$(S). (2) For a single closed atomic shell of Ar atoms the spectral shift for the (C) site is $\delta\nu$ = 0.32−0.26 eV over T = 5−30 K. For the (S) site $\delta\nu$ = 0.12−0.11 eV over T = 5−30 K. (3) The line widths at T < 30 K also obey the relation Γ(C) > Γ(S). (4) Above T > 30 K specific ground state (C) ⇄ (S) dynamic isomerization is manifested in the spectrum. The spectral observables for the initially prepared (C) and (S) Xe atom substitutional sites practically coincide.

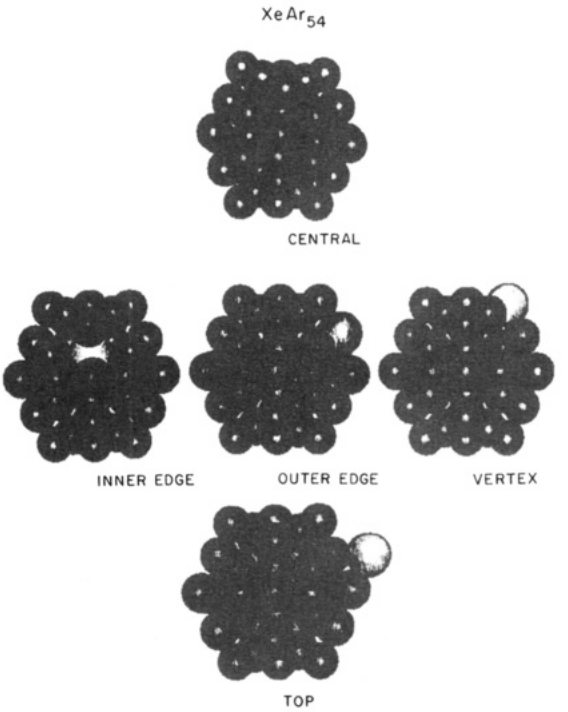

Figure 3. Snapshots of the five distinct substitutional (C), (I), (O), (V), and (T) sites of Xe in $XeAr_{54}$.

Proceeding to $XeAr_{54}$ (Figure 3), the initial ground-state substitutional Xe atom configurations (Table 1) are[1] (C) central position, (I) inner edge, (O) outer edge, and (V) vertex. In addition, the (T) top Xe adsorbed on the cluster surface was studied. The (O), (V), and (T) sites correspond to distinct

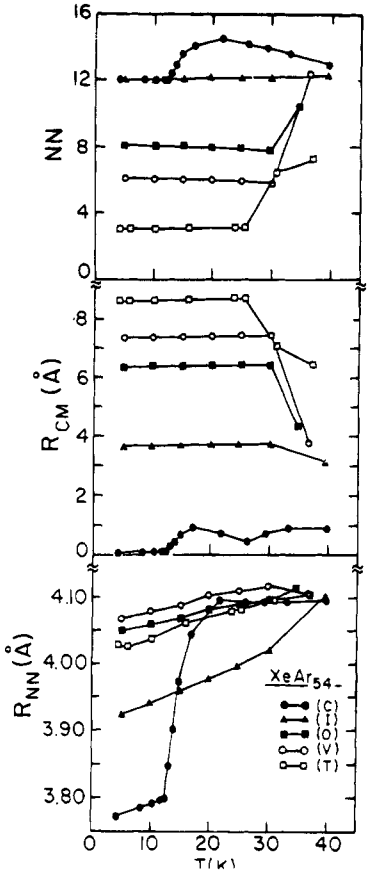

Figure 4. Temperature dependence of the structural parameters NN, R_{CM}, and R_{NN} for the different initial Xe substitutional sites (C), (I), (V), (O), and (T) (marked on figure) in $XeAr_{54}$.

surface states. The ground-state nuclear parameters for the (C) site reveal a marked configurational change at $T = 13$ K (Figure 4), where R_{NN} abruptly increases from 3.8 Å at 12 K to 4.0 Å at 15 K and concurrently NN increases from 12 at 12 K to 15 at 15 K. These new dramatic structural effects in the heterocluster reflect ground-state configurational dilation around the (C) site in a heterocluster which is occupied by a substitutional atom whose radius exceeds that of the host atoms. This configurational change is specific for the (C) site. The structural parameters for the (I), (O), and (V) sites exhibit a smooth temperature dependence at $T < 35$ K and no evidence for ground-state configurational dilation around these sites is exhibited (Figure 4). The configurational parameters for the T site exhibit an abrupt change at $T > 25$ K (Figure 4). This pattern reflects surface melting.[79] The simulated spectra of $XeAr_{54}$ clusters (Figures 5 and 6) reflect the configurational dilation around the (C) sites and reveal the spectroscopic manifestations of the atomic shell structure.

(1) At low T ($\simeq$10 K) the spectra show a characteristic nuclear shell structure with the hierarchy $\delta\nu$(C) > $\delta\nu$(I) > $\delta\nu$(O) > $\delta\nu$(V) > $\delta\nu$(T). This pattern is in accord with the decrease of the structural R_{NN} and NN parameters for these sites (Figure 4) at low T (5−13 K).

(2) With increasing T in the range 10−20 K the spectral shift of the (C) site decreases sharply (Figure 5). From the T dependence of the spectral shift (Figure 6), the break in $\delta\nu$ is exhibited at $T \geq 13$ K, which coincides with the change in the structural parameters (Figure 4).

(3) In contrast to the interesting behavior of the spectroscopy of the (C) site, the behavior of Xe in the (I), (O), and (V) sites is "normal" over the temperature range up to 35 K. This is evident from the smooth T dependence of $\delta\nu$ and Γ (Figure 6), in accord with the pattern of R_{NN} and NN for these sites (Figure

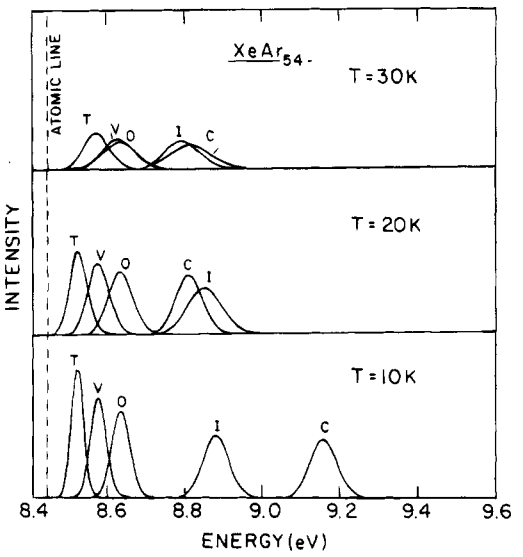

Figure 5. Temperature dependence and site specificity of the line shapes of $XeAr_{54}$ cluster. The substitutional sites (Table 1) are marked on the individual spectra.

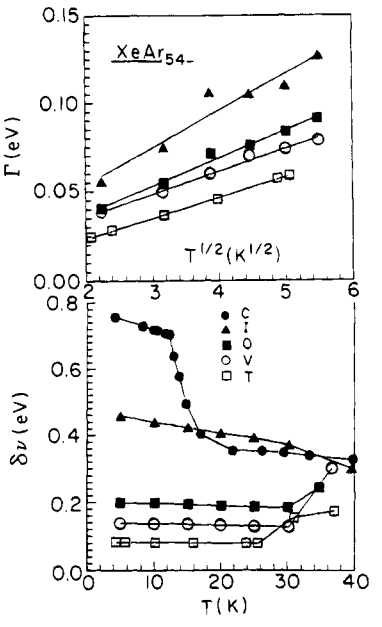

Figure 6. Temperature dependence of $\delta\nu$ and Γ according to eqs 4.3 and 4.4 for different initial Xe substitutional sites (marked on the figure) in $XeAr_{54}$.

4). For these sites up to 35 K $\delta\nu$ and Γ (Figure 6) obey eqs 4.3 and 4.4. The parameters B (<0) increase in the order (I) < (O) < (V) < (T), reflecting the decrease of the temperature coefficient with decreasing $\delta\nu$.

(4) The line widths roughly follow the order of the spectral shifts.

(5) For the top atom the spectral behavior is smooth, up to 26 K (Figures 5 and 6). Above 27 K the spectral shift for the top Xe atom increases with increasing T, reflecting the diving of this atom (in the ground state) into the cluster. This is the onset of the surface melting of the cluster (Figure 6), which can be monitored by electronic spectroscopy of the impurity atom.

(6) At low temperatures (10 K) the spectral shift of the central atom is 0.72 eV. Thus two nuclear shells are required to accomplish the large spectral shift.

We now proceed to the spectra of $XeAr_{146}$. There are seven substitutional sites (Table 1):[1] (C) center; (1), (2), and (3) inequivalent sites in the inner sphere; (4), (5), and (6) inequiva-

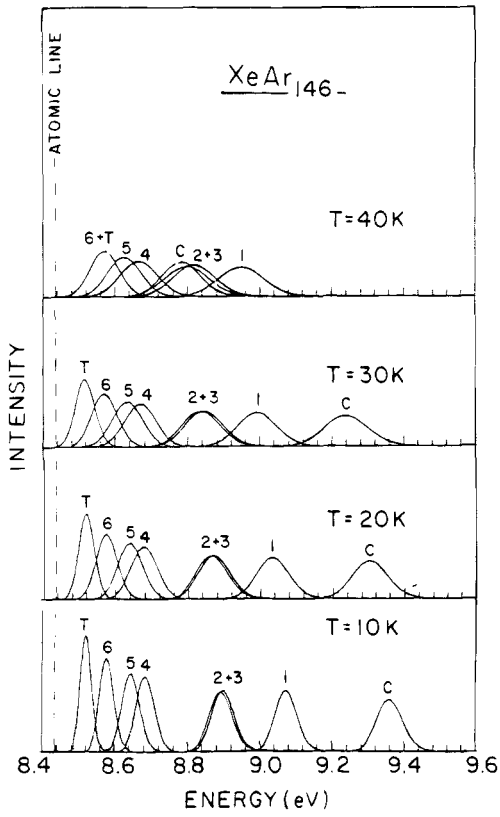

Figure 7. Temperature dependence and site specificity of the line shapes of $XeAr_{146}$ clusters. The substitutional sites (Table 1) are marked on the individual spectra. The dashed vertical line represents the bare Xe atom transition.

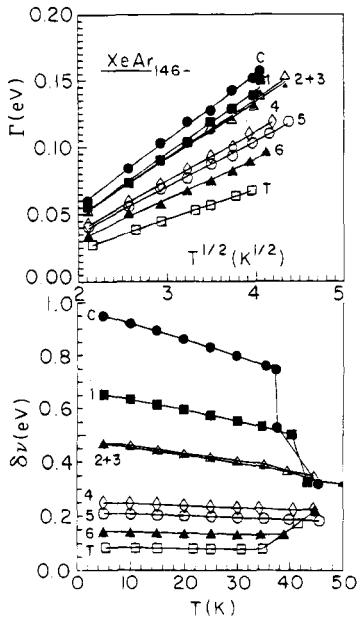

Figure 8. Temperature dependence of $\delta\nu$ and Γ according to eqs 4.3 and 4.4 for different initial Xe substitutional sites (marked on the figure) in $XeAr_{146}$.

lent sites on the outer sphere. In addition, we have studied the (T) top atom. There are four interior sites, i.e., (C), (1), (2), and (3) and four surface sites: the substitutional (4)−(6) sites and the (T) site. From the simulated absorption spectra (Figure 7) and the temperature dependence of $\delta\nu$ and Γ (Figure 8) we conclude the following: (1) Spectroscopic manifestation of the hierarchy of the nuclear shell structure is now observed over the broad T domain up to 35 K, where $\delta\nu(C) > \delta\nu(1) > \delta\nu(2) \simeq \delta\nu(3) > \delta\nu(4) > \delta\nu(5) > \delta\nu(6) > \delta\nu(T)$. (2) The central

TABLE 4: Temperature Onsets (K) of Various Isomerization Processes in $XeAr_N$: Configuration Dilation around the (C) Site (T_c) and Surface Melting (T_{SM})

N	T_c	T_{SM}
54	13	>25
146	37	35
199	>35; <40	37
204	>25; <30	

atom exhibits the largest spectral shift $\delta\nu = 0.90-0.76$ eV over $T = 10-35$ K. (3) Above 37 K, $\delta\nu$(C) is considerably reduced (Figure 8). Again, the ground-state structural parameters R_{NN} and NN considerably increase. The marked reduction of $\delta\nu$-(C) is due to ground state configurational dilation around the (C) site of Xe. (4) Over the "normal" region, i.e., $T \leq 37$ K for the (C) site, $T \leq 40$ K for the (1)−(6) sites, and $T \leq 35$ K for the (T) site, the temperature dependence of $\delta\nu$ and Γ is well accounted for by eqs 4.3 and 4.4 (Figure 8). (5) $\delta\nu$ for the (T) site increases with increasing temperature above 35 K (Figures 7 and 8). This abnormal behavior is associated with surface melting. (6) Simulations for the "amorphous" $XeAr_{146}$ cluster at 25 K (quenched to $T = 25$ K from an equilibrated "molten" cluster at $T = 55$ K) give $\delta\nu = 0.52$ eV. This value of $\delta\nu$ is considerably lower than $\delta\nu = 0.83$ eV for an equilibrated cluster at $T = 25$ K. The line width of the amorphous cluster is close to that of the equilibrated cluster, not exhibiting marked inhomogeneous broadening effects.

VII. Configurational Changes in $XeAr_N$ Heteroclusters

The excited-state energetics of $XeAr_N$ clusters is extremely sensitive to the microenvironment of the Xe atom. Structural data provide information on temperature induced configurational changes in $XeAr_N$ heteroclusters. The combination of the structural and spectroscopic data will make contact with experimental reality. This allows for the spectroscopic identification of cluster configurational changes and isomerization processes by the interrogation of the temperature dependence of the energetics of the extravalence electronic excitation. We were able to identify three temperature induced "transitions" in $XeAr_N$ clusters (Table 4).

(1) The onset of (C) $\rightleftarrows$ (S) dynamic isomerization of the Xe atom in $XeAr_{12}$, occurring at $T_I \simeq 30$ K.

(2) Configurational dilation around the (C) site with an onset at $T = T_c$, which was identified for $N = 54$ and 146. This configurational change was also observed in large clusters ($N = 199$, 206), which involve an open atomic shell. The specific cluster size dependence of T_c is nonmonotonous.

(3) Surface melting. The temperature T_{SM} for surface melting increases with increasing the cluster size.

These data will be of importance for the understanding of isomerization dynamics of heteroclusters and for the interpretation of experimental finite temperature spectroscopic results.[58-60]

VIII. A Structure−Spectra Relationship

It will be instructive to quantify the effect of the cluster microenvironment of the guest Xe atom on the electronic spectrum. The $Xe^*(^3P_1)-Ar$ interactions are dominated by short-range overlap-exchange electronic repulsions, which are expected to depend exponentially on the $Xe^*(^3P_1)-Ar$ separation. Guided by these simple considerations we advance the relationship

$$\delta\nu = a(\mathrm{NN}) \exp[-\gamma R_{NN}] \qquad (8.1)$$

where a is a constant (in energy units) and γ is a (range parameter) constant. This relationship is expected to account for the site specificity, for the smooth temperature dependence

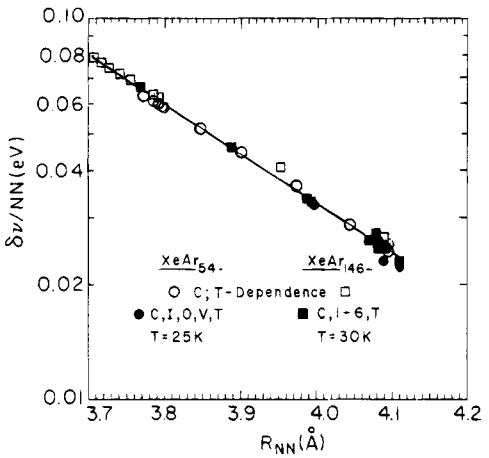

Figure 9. Analysis of the site specificity and temperature dependence of $\delta\nu$ according to eq 8.1. The temperature dependence (T = 10–40 K) for the (C) Xe substitutional site for N = 54 (○) and for N = 146 (□). The site specificity for the five Xe substitutional sites of $XeAr_{54}$ at T = 25 K (●) and for the eight Xe substitutional sites of $XeAr_{146}$ (■) at T = 30 K. Note the universality of this cluster size invariant relation.

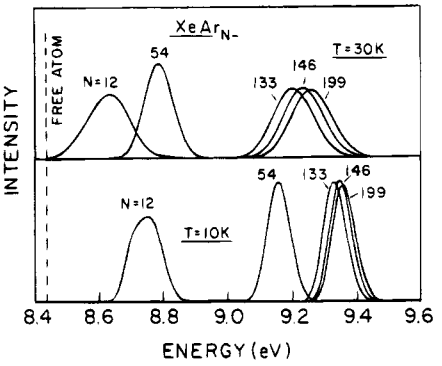

Figure 10. Cluster size and temperature dependence of the line shapes for the (C) Xe substitutional site. The dashed vertical line represents the bare Xe atom excitation.

(at $T < T_c$) and also for the temperature induced configurational changes of the spectral shift (at $T > T_c$). As is apparent from the linear plot of ln[$\delta\nu$/NN] vs R_{NN} (Figure 9), all the data for distinct Xe substitutional sites and for the temperature dependence of $\delta\nu$ for N = 54 and 146 fall on a universal curve for all cluster sizes, in accord with eq 8.1. The parameters are $a = (6.2 \pm 0.6) \times 10^3$ eV and $\gamma = 3.05 \pm 0.05$ Å^{-1}, being cluster size independent. Equation (8.1) provides a physically transparent and useful structure–spectra relationship.

IX. Spectra of Large Clusters

To make contact with the experimental spectroscopic data of Möller et al.,[58–60] the spectra of "large" clusters (N = 130–206) were simulated. Typical data for the (C) Xe occupied site are given in Figure 10 and in Table 5, while information on site-specific spectral shifts and line widths are summarized in Tables 5 and 6. Note the following results:

(1) Size effects on $\delta\nu$ and Γ for the (C) site of large clusters at a constant temperature ($T < T_c$). These are small, i.e., the spread of $\delta\nu$ is ~3% and the spread of Γ is ~10%. Accordingly, the effects of inhomogeneous broadening on the (C) site at $T < T_c$ are small. Of course, for $T > T_c$ (with T_c being size dependent), a large inhomogeneous broadening will be exhibited.

(2) The temperature dependence of $\delta\nu$ and Γ for the (C) site obeys relations (4.3) and (4.4) (see Figure 11 for N = 199). The parameters A, B, and C at $T < T_c$ exhibit only a weak size dependence.

(3) Atomic shell structure. Again, a hierarchy of absorption bands, due to different sites, emerges (Table 5).

Some generalization of cluster size invariant spectral shifts can be made on the basis of the data of Table 5:

(4) The top atom absorption is cluster size independent. However, the spectroscopic observation of the top Xe atom at experimentally realistic temperatures may be precluded by surface melting (Table 4).

(5) Xe substitutional surface sites exhibit $\delta\nu$ = 0.11–0.27 eV for a broad cluster size domain N = 54–206. The energetic

TABLE 5: Atomic Shell Structure Effects on the Spectral Shifts (eV) of $XeAr_N$ Clusters at Several Temperatures ($T < T_c$)

	$N = 54^a$		$N = 146^a$		$N = 199^a$		experiment[b] and assignment	
	T = 10 K	T = 10 K	T = 30 K	T = 35 K	T = 30 K	T = 35 K	$N = 150^d$	$N = 200^e$
central	0.72 (C)	0.92 (C)	0.80 (C)	0.76 (C)	0.83 (C)	0.78 (C)		0.78 (C)
		0.64 (1)	0.55 (1)	0.53 (1)	0.59 (1)	0.56 (1)		0.65 (I)
interior	0.44 (I)	0.46 (2)	0.41 (2)	0.39 (2)	0.48 (2)	0.42 (2)		0.45 (I)
		0.45 (3)	0.40 (3)	0.38 (3)	0.44 (3)	0.39 (3)		
					0.35 (5)			
		0.25 (4)	0.23 (4)	0.23 (4)	0.25 (6)	0.27 (6)		
surface	0.20 (O)	0.21 (5)	0.20 (5)	0.19 (5)	0.16 (7)	0.15 (7)	0.25 (S)	0.27 (S)
	0.14 (V)	0.14 (6)	0.13 (6)	0.13 (6)	0.12 (8)	0.11 (8)		
top	0.083	0.084		0.078				

[a] Simulated data. [b] References 58–60. [c] (C) central, (S) substitutive surface, (I) interior. [d] Crossed (Xe + Ar_N) beams experiment.[58,60] [e] 0.01% Xe + Ar expansion.[58]

TABLE 6: Line Widths Site-Specific Γ (eV) of $XeAr_N$ Clusters at Several Temperatures

	$N = 54^a$	$N = 146^a$			$N = 199^a$			experiment[b] and assignment[c]		
	T = 20 K	T = 20 K	T = 30 K	T = 35 K	T = 20 K	T = 30 K	T = 35 K	$N = 150^d$	$N = 200^e$	$N = 500^e$
central	0.082	0.12	0.14	0.15	0.12	0.15	0.17		0.10 (C)	0.12 (C)
interior	(I) 0.11	(1) 0.11	(1) 0.13	(1) 0.14			(1) 0.14			
		(2) 0.10	(2) 0.12	(2) 0.13			(2) 0.15		0.14 (I)	0.16 (I)
		(3) 0.10	(3) 0.12	(3) 0.13			(3) 0.14		0.18 (I)	0.21 (I)
surface	(O) 0.086	(4) 0.084	(4) 0.10	(4) 0.11			(4) 0.14			
	(V) 0.067	(5) 0.079	(5) 0.096	(5) 0.10			(5) 0.13	0.11 (S)	0.16 (S)	0.12 (S)
		(6) 0.068	(6) 0.082	(6) 0.089			(6) 0.12			
							(7) 0.10			
							(8) 0.090			
top	0.056	0.051	0.064							

[a] Simulated data. [b] References 58–60. [c] (C) central, (I) interior, (S) surface. [d] Crossed Xe + Ar_N beams. [e] 0.01% Xe + Ar expansion.

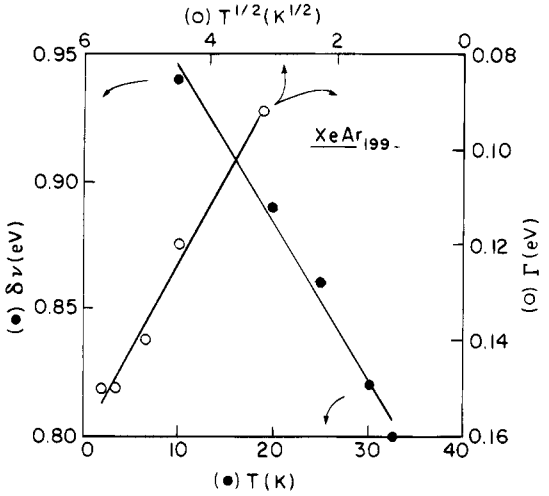

Figure 11. Temperature dependence of $\delta\nu$ and Γ for the (C) Xe substitutional site in $XeAr_{199}$ according to eqs 4.3 and 4.4.

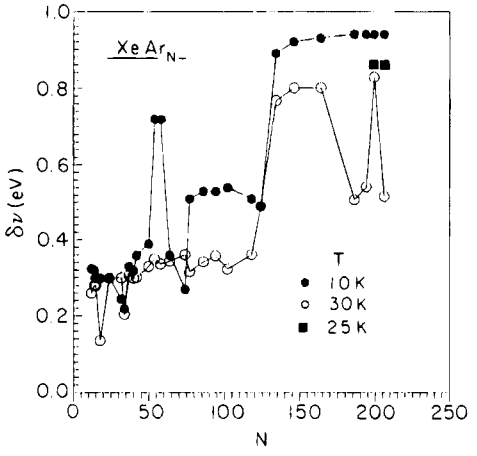

Figure 12. Size dependence of the spectral shifts for the (C) Xe substitutional site in $XeAr_N$ ($N = 12-206$) clusters in the temperature range 10–30 K.

spread of Γ for the surface states (~0.16 eV) somewhat exceeds the calculated line widths (Table 6). Accordingly, inhomogeneous broadening for surface states, which is due to distinct sites, involves a contribution of ~0.16 eV (i.e., ~ 1.0–1.5Γ).

(6) Spectra of other interior sites reveal a "gap" between the (C) site and the interior sites of the outer shells (1)–(3). The spread of the energies of the interior states will be marked (>0.2 eV) and the energy spacing between the lowest energy interior excitation and the highest surface excitation will be smaller than the line width at $T = 30-35$ K. Inhomogeneous broadening effects due to different interior sites will be quite severe.

X. Cluster Size Dependence of Absorption Spectra of the (C) Site

We simulated the spectral line shapes for the (C) Xe-atom configuration over the range $N = 12-206$ at $T = 10$ K, which is of methodological interest and at 30 K, being of practical interest. Figures 12 and 13 portray the size dependence of the spectral shifts and the line widths. The 10 K $\delta\nu$ data show the following:

(1) Highly specific size effects in the range $N = 12-64$, with a "magic number" for $\delta\nu$ at $N = 54$.

(2) Two flat regions of $\delta\nu$ vs N, i.e., $64 \leq N \leq 120$ ($\delta\nu \sim 0.5$ eV) and $N > 130$ ($\delta\nu \simeq 0.9$ eV) are exhibited. The latter high value of $\delta\nu$, which exceeds the experimental spectral shift in the low-temperature solid,[61-65,113] may manifest the effect of the low-temperature icosahedral structure on $\delta\nu$ (section XI.C).

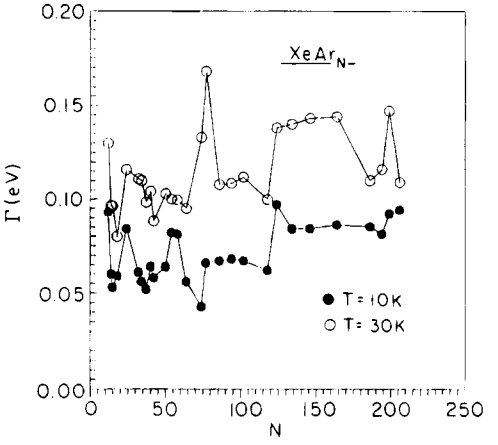

Figure 13. Size dependence of the line widths for the (C) Xe substitutional site in $XeAr_N$ ($N = 12-206$) clusters at $T = 10$ and 30 K.

(3) The onset of the large spectral shift for $N \gtrsim 130$ reflects the necessary buildup (although not complete closure) of the second layer.

(4) The large spectral shift for $N \geq 130$ is practically size independent.

(5) The spectral shifts for surface sites at $T = 10$ K are $\delta\nu = 0.08-0.20$ eV for the entire size domain $N = 12-206$, being considerably lower than the $\delta\nu$ for the (C) site.

What we need to make contact with experiment are the higher temperature ($T = 30$ K) results, which reveal the following features of the (C) site:

(6) The low-T specific spectral shifts in the range $13 \leq N \leq 120$ are eroded.

(7) The spectral shifts in the range $13 \leq N \leq 120$ are low, being $\delta\nu \simeq 0.26-0.36$ eV.

(8) An onset of a high $\delta\nu$ is exhibited at $N \simeq 130$.

(9) For $N \geq 130$ high values of $\delta\nu \simeq 0.8$ eV are exhibited at 30 K for those clusters which satisfy $T_c > 30$ K (Table 4).

(10) For those cluster sizes where $T_c < 30$ K, drops of $\delta\nu$ will be exhibited. Thus the configurational dilution around the (C) site results in the oscillations of $\delta\nu$ vs N for $N > 130$ at 30 K. At 25 K (still a "reasonable" experimental temperature) this oscillation will be eroded and $\delta\nu$ maintains a high value.

(11) For the spectra of the (C) site at 25–30 K we expect that (i) for "large" clusters a size distribution of clusters around average values of $N = 150-200$ will exhibit the high $\delta\nu$ (0.8 eV) absorption for the (C) site; (ii) for clusters with $N < 120$ or so, the largest $\delta\nu$ will not exceed 0.35 eV.

To put some order into the results of Figure 12 we have calculated the size dependence of the structural parameters R_{NN} and NN. As is apparent from Figure 14 all the $\delta\nu$ data for the (C) site for $N = 12-206$ at the two temperatures $T = 10$ K and $T = 30$ K fall on the universal plot predicted by eq 8.1, which accounts well for the structure–spectrum relationship over a broad size domain.

XI. Confrontation between Theory and Experiment

Möller and his colleagues[58-60] applied energy and time-resolved fluorescence methods with synchrotron radiation excitation to study the electronic spectroscopy and the excited state dynamics of the two lowest $^1S_0 \rightarrow {}^3P_1$ and $^1S_0 \rightarrow {}^1P_1$ excitations of Xe in $XeAr_N$ ($N = 1-5000$) clusters. Möller et al.[58-60] have observed three absorption bands for the lowest Xe-($^1S_0 \rightarrow {}^3P_1$) transition which were assigned by them to the excitation of the Xe atom in the interior of the cluster, in a substitutional position inside the cluster surface and on the top of the cluster. In what follows we shall confront the results of

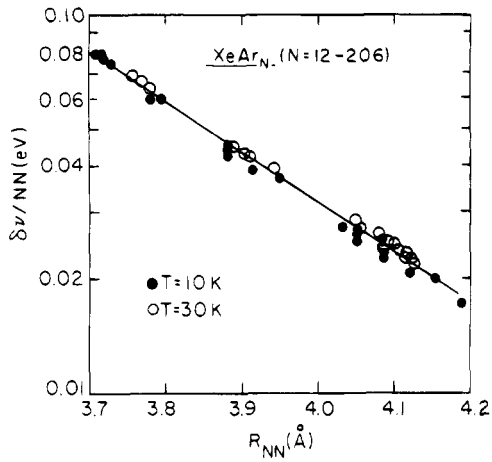

Figure 14. Analysis of the cluster size dependence and temperature dependence of $\delta\nu$ for the (C) Xe substitutional site in $XeAr_N$ (N = 12−206) clusters according to eq 8.1. The parameters a and γ are identical (within 5%) with those of Figure 8.

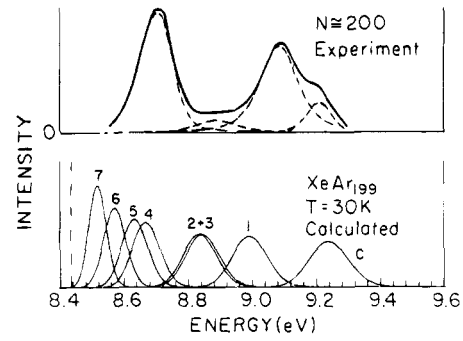

Figure 15. Comparison between the calculated site-specific line shapes of $XeAr_{199}$ at T = 30 K (lower panel) and the experimental spectrum[58] of $XeAr_{200}$ (upper panel). The calculated line shapes are labeled by the specific sites: C = central Xe substitutional sites, 1−4 interior Xe substitutional sites, and 5−8 surface Xe substitutional sites. The experimental spectrum obtained from the expansion of Xe (0.01%) is decomposed into separate (dashed line) Gaussians, which represent site specific excitations.[58] The vertical dashed line is the bare Xe atom excitation.

our simulations for the Xe($^1S_0 \rightarrow {}^3P_1$) transition in $XeAr_N$ (N = 12−206) clusters with experimental reality[58-60] for the identification of the site-specific electronic excitations. We shall be able to provide compelling evidence for the spectroscopic identifications of the following five Xe substitutional sites: the (C) and (S) sites in small ($N \simeq 12$) clusters, the (C), interior and substitutional surface sites in large ($N \geq 130$) clusters. No evidence was obtained for the existence of the (T) site. Notwithstanding these successes, we have failed to identify one prominent absorption band with $\delta\nu$ = 0.63−0.66 eV observed[58-60] in small- and medium-sized N = 10−35 clusters. The present analysis of the structure−spectra relations will provide a critical scrutiny for the accuracy and reliability of our simulations for the rather detailed elucidation of excited state energetics of these elemental heteroclusters.

(XI.A) (C) Site in Large Clusters. The comparison between theory and experiment for the spectroscopic observables requires two sources of experimental information. (i) The cluster average size, which was estimated by Möller et al.[58-60] from experimental scaling relations.[26] (ii) The cluster temperature which is approximately inferred from electron diffraction experiments[26,114,115] and from evaporative cooling models[116,117] for neat clusters. The experimental information[26,114,115] for the temperature of Ar_N clusters synthesized by supersonic expansion of Ar from a circular (50−400 μm) nozzle is $T = 27 \pm 3$ K for $N \simeq 40$ and $T = 34 \pm 3$ K for $N \simeq 150$. In accord with these data, Möller et al.[58-60] have assigned the temperature T = 25−35 K to the $XeAr_N$ clusters. Our simulations for the structure and spectra of the (C) site for large $N \geq 130$ clusters in this "experimentally reasonable" T = 25−35 K domain (sections VI and IX) reveal that (i) this temperature range essentially corresponds to $T < T_c$ and (ii) the excitation energy of the (C) site is high, $\delta\nu$ = 0.76−0.83 eV.

The experimentally highest energy excitation of the Xe($^1S_0 \rightarrow {}^3P_1$) manifold in large N = 200 and N = 500 $XeAr_N$ clusters, which is characterized by $\delta\nu$ = 0.76−0.78 eV[58-60] for both cluster sizes, is assigned to the Xe excitation at the (C) site, as is apparent from Figure 15 where we compare the experimental spectrum of $XeAr_{200}$ with the simulated site specific spectra of $XeAr_{199}$ at T = 30 K. The agreement between theory and experiment for $\delta\nu$ (Table 5) is excellent. The excitation energy of the (C) site in large clusters is expected to be nearly cluster size independent (section X), in accord with the experimental results.[58-60] The experimental line widths[58] of the (C) site are close to, but slightly lower than, the simulated line widths (Table 6). In any case, the effects of inhomogeneous broadening for the (C) site, due to the distribution of cluster sizes, is minor. On the basis of this rather impressive agreement between theory and experiment for $\delta\nu$ and Γ, we infer that the assignment of the (C) Xe-atom occupied site in large $XeAr_N$ clusters is conclusive. The original assignment[58] of the highest energy electronic excitation to an interior site has to be slightly modified to refer to the specific (C) site, an amendment which is acceptable to Möller et al.[59,60]

(XI.B) The Cluster Temperature. The temperature dependence of $\delta\nu$ and Γ can serve, in principle, as an internal thermometer for the determination of the cluster temperature. From the experimental and theoretical $\delta\nu$ data for the (C) site (Table 5) we estimate the temperature of the $XeAr_N$ ($N \simeq$ 146−200) clusters, T = 30−35 K. This spectroscopic determination is in excellent agreement with the experimental estimate[58-60] of the cluster temperature. The experimental and calculated line widths (Table 6) somewhat underestimate the cluster temperature, yielding $T \simeq 20$ K, where $\delta\nu$ is too large, i.e., $\delta\nu$ = 0.86 eV for N = 146 and $\delta\nu$ = 0.89 eV for N = 199. In spite of this slight inconsistency, we shall assert that a satisfactory picture for the (C) site at $T \simeq$ 30−35 K emerged from our analysis of the (C) site.

(XI.C) A Comparison between Cluster and Solid-State Spectra. Möller et al. have compared[58-60] the spectrum of the highest energy (C) site for $N > 200$ with the spectrum of Xe in an Ar matrix. In view of the availability of detailed experimental information on cluster spectra,[58-60] together with the present accurate theoretical results on the temperature dependent line shapes, a more detailed comparison between the (C) site and condensed-phase Xe/Ar spectroscopy will be instructive. The spectra of matrix isolated Xe in Ar[61-65] was obtained at low temperatures (T = 4 K) and cannot be readily compared to the $XeAr_N$ cluster spectra at T = 30−35 K. Fortunately, experimental absorption spectroscopy data are available for Xe (1 ppm) impurity in thick (~1 cm) Ar crystals over the temperature range T = 33−80 K.[61,113] We have compared in Figure 16 the spectral shifts of the Xe/Ar solid at T = 33−35 K with the Xe (C) site in $XeAr_N$ clusters at the same temperature (section XI.B). The overall size dependence of $\delta\nu$ is weak, changing over the range of 0.01 eV. There is a small, but definite, decrease of $\delta\nu$ with increasing N in the range $N >$ 1500, which may reflect structural change around the (C) site. A possible candidate is the structural change from the icosahedral cluster structure toward the bulk face center cubic (FCC) structure.[106,118] The $\delta\nu$ values for very large (N = 1500−5000) clusters seem to converge smoothly to the bulk spectrum at T

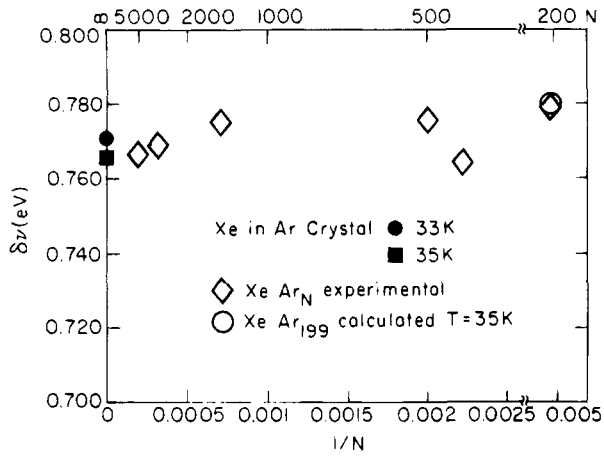

Figure 16. Cluster size dependence of the experimental $\delta\nu$ data for the (C) Xe substitutional site in $XeAr_N$ ($N = 200-5000$) clusters,[58,60] together with $\delta\nu$ of Xe in crystalline Ar at $T = 33$ and 35 K.[113] We have also added the simulated result for $XeAr_{199}$ at $T = 35$ K.

$= 33-35$ K (Figure 16). For large heteroclusters, whose structure is size invariant, one expects a CSE for the spectral shift of an electronic transition, whose blue spectral shift is dominated by a short-range repulsive interaction, to be in the form[24,104] $\delta\nu(N) = \delta\nu(\infty) + A/N$, where A is a numerical constant. This CSE reflects the role of long-range dispersive contributions to the spectral shift, which reduce $\delta\nu$ with increasing the cluster size.[24,104] For a rough estimate of the parameter A we utilize the spectral shifts of the electronic transition of an aromatic molecule[41-56] (with an oscillator strength $f \simeq 0.1$) in Ar clusters[24] which gives $A = 0.5$ eV and assume that $A \propto f$. Accordingly, for the Xe($^1S_0 \rightarrow {}^3P_1$) transition ($f = 0.3$ [119]) we expect that $A \simeq 1.5$ eV. This estimate is in accord with the weak size dependence of $\delta\nu$ for these $XeAr_N$ clusters (Figure 16). However, the small changes in $\delta\nu$ prohibit a quantitative analysis of the spectral shift.

The close agreement between the numerical values of the simulated and experimental $\delta\nu$ data for the Xe (C) site in "large" $N = 146$, 199 clusters at $T = 30-35$ K and the bulk Xe/Ar spectra at the same temperature, is somewhat surprising in view of the structural difference between the icosahedral cluster structure and the bulk FCC structure. The number of nearest neighbors is identical for both structures; however, one expects the nearest-neighbor Xe−Ar distances to be different in both cases, with R_{NN} for the cluster to be shorter than for the FCC bulk. This difference in R_{NN} will be manifested at low temperatures. Accordingly, we expect on the basis of eq 8.1, that $\delta\nu$ in the low-temperature cluster will be lower than in the bulk. In the following analysis of low-temperature cluster spectra we shall use the results of classical simulations at $T =$ 10 K, where quantum corrections for $XeAr_N$ are expected to be minor.[120] Subsequently, the classical spectral data simulated at $T = 10$ K will be compared with the low temperature $T = 4$ K experimental results. The low-temperature simulated spectral shift for the Xe (C) site in the icosahedral $XeAr_{199}$ cluster is $\delta\nu = 0.95$ eV at $T = 10$ K (Figure 11), being considerably higher than the experimental spectral shift in the solid[61-65] $\delta\nu = 0.76-0.78$ eV at $T \simeq 4$ K. The enhancement of the low-temperature $\delta\nu$ in the cluster relative to the bulk can be rationalized on the basis of relation 8.1, which yields $\delta\nu(C)/\delta\nu(BULK) = \exp[\gamma(R_{CC}^{(BULK)} - R_{CC}^{(C)})]$, where (C) and (BULK) refer to the (C) site in large clusters and to the bulk solid, respectively. Accordingly, taking $\delta\nu(C)/\delta\nu(BULK) = 1.25$ we estimate $R_{CC}^{(BULK)} - R_{CC}^{(C)} = 0.08$ Å at low temperatures. This rough estimate of the difference between the Xe−Ar distances is consistent with the value $R_{CC}^{(BULK)} - R_{CC}^{(C)} \simeq 0.15$ Å obtained from MD simulations for $XeAr_{146}$ ($T = 10$ K), which give

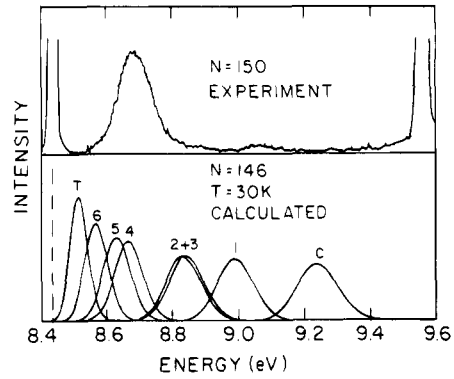

Figure 17. Comparison between the calculated Xe site-specific line shapes of $XeAr_{146}$ at $T = 30$ K (lower panel) and the experimental spectrum of $XeAr_{150}$ prepared in a crossed beam experiment of Xe + Ar_N.[59,60] The calculated line shapes are labelled by the specific sites (Table 1). The horizontal dashed line is the bare Xe atom excitation.

$R_{CC}^{(C)} = 3.73$ Å, together with a recent simulation result $R_C^{(BULK)} = 3.88$ Å obtained by Fraenkel and Haas for Xe in FCC annealed bulk Ar matrix at 1 K,[121] which is based on the same potential parameters as used herein. Further work on this interesting comparison between cluster and bulk spectra will be of interest.

(XI.D) Identification of Surface and Interior Sites in Large Clusters. Experimental crossed-beam experiments,[58-60] which utilize the crossing of an atomic beam of Xe with a cluster beam of Ar_N, allow us to conduct spectroscopy of surface states of the Xe atom in a substitutional surface or a (T) configuration. In Figure 17 we confront the experimental spectrum of a $XeAr_N$ ($N = 150$) prepared[60] in a Xe + Ar_N crossed-beam experiment, with the simulated site specific spectra of $XeAr_{146}$ at $T = 30$ K. This preparation method favors the production of surface impurity sites.[74] A remarkable feature of this experimental spectrum (Figure 17) is the 'spectroscopic desert' in the range 8.8−9.4 eV. The contribution of the (C) site and the interior (1), (2), and (3) sites is negligible. The prominent experimental absorption band which peaks at 8.7 eV ($\delta\nu = 0.16$ eV) (Figure 17) is assigned to the superposition of excitations of the Xe substitutional surface sites (4), (5), and (6), with a major contribution from the surface site (4), as is evident from the analysis in Figure 17. The experimental line width of the absorption band $\Gamma = 0.12$ eV exceeds the calculated line widths (Table 6), reflecting the effects of inhomogeneous broadening. We note that the excitation of the (T) site is missing (Figure 17). This is presumably due to the "diving effect" of the Xe atom into the first surface layer cluster, which is caused by surface melting. Simulations and analysis of the dynamics of Xe + Ar_N collisions will be presented in the future.[122]

We are now able to provide assignments of substitutional surface sites (sites (4)−(6) for $N = 146$ and sites (4)−(7) for $N = 199$) and of interior sites (e.g., sites (1)−(3) for $N = 146$ and for $N = 199$), which are exterior to site (C), in large clusters prepared in Xe(0.01%) + Ar supersonic expansions. The band at $\delta\nu = 0.27$ eV observed in $XeAr_{200}$ and $XeAr_{500}$[58] is assigned to substitutional surface sites (Figure 15). The agreement between the simulated and the experimental $\delta\nu$ values (Table 5 and Figure 15) is satisfactory. The experimental line width $\Gamma = 0.16$ eV contains a contribution of inhomogeneous broadening due to distinct interior sites. Again, no evidence was obtained for the existence of a (T) site, which is presumably precluded by surface melting. Finally, the band at $\delta\nu = 0.66$ eV and the broad band at $\delta\nu = 0.46$ eV in $XeAr_{200}$ (Figure 15) are assigned to interior sites. The best agreement (Table 5) is achieved for the interior sites (1) and (2), respectively.

In view of the weak cluster size dependence of $\delta\nu$ for the

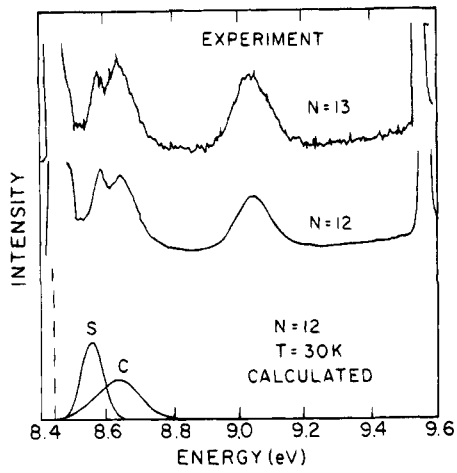

Figure 18. Comparison between the calculated Xe-substituted site-specific line shapes of $XeAr_{12}$ at $T = 30$ K (lower panel) and the experimental spectra of $XeAr_{12}$ and $XeAr_{13}$ (the middle and upper spectra) obtained from the expansion of Xe (0.001−0.01%) + Ar.[59,60] The vertical dashed line is the bare Xe atom excitation.

substitutional surface sites (section IX), we expect that the $\delta\nu \simeq 0.26$ eV band over the entire size domain $N = 200-5000$[58] corresponds to those substituted surface sites. Also, the energetics of the interior sites (1)−(3) is cluster size independent and we assign the $\delta\nu = 0.65-0.66$ eV band for $N = 200-5000$ to the interior, i.e., the (1) and (2), site(s).

The inhomogeneous broadening of the excitations of substitutional surface and of interior sites in large clusters will depend on the following: (i) The distribution of the $XeAr_N$ cluster sizes, which depends on the supersonic beam conditions. We have shown that some distinct Xe sites, i.e., the (C) configuration, the substitutional surface and the interior (1)−(3) sites exhibit a weak size dependence, providing only a moderate contribution (~0.1−0.2 eV) to inhomogeneous broadening. (ii) Distribution of distinct Xe trapping sites, which do not communicate at sufficiently low temperatures, e.g., $T < T_I$ for (C) $\rightleftarrows$ (S) isomerization for $N = 12$ or $T < T_{SM}$ for the conversion of (T) to substitutional surface sites. This distribution of static structural isomers depends on the cluster preparation conditions. The rationalization of the dominance of Xe substitutional surface sites in Xe + Ar_N crossed-beam cluster preparation is self-evident. We have simulated site-specific spectra but did not yet succeed to simulate a superposition of isomers, which will reproduce the experimental abundance of distinct Xe sites in $XeAr_N$ clusters prepared by Xe(0.01%) + Ar expansion.

Our simulations show that a large spectral shift of $\delta\nu \simeq 0.8$ eV at 30−35 K can be realized for the (C) configuration in a $XeAr_N$ cluster with three or more atomic shells. Accordingly, the high-energy (C) site ($\delta\nu \simeq 0.8$ eV) will be realized in the size domain $N > 130$ for the experimentally realistic temperatures $T = 30-35$ K (section XI.B). Concurrently, the interior (e.g., (1) + (2)) and substitutional surface sites were identified for these large clusters. For small ($N < 120$) clusters the excitation energies of the (C) sites are expected to be considerably lower (section X and Figure 12).

(XI.E) $XeAr_{12}$ Spectrum. The experimental spectra of small $XeAr_N$ ($N = 10-20$) clusters exhibit two bands at $\delta\nu = 0.12$ eV and $\delta\nu = 0.21$ eV (Figure 18). These two bands are assigned to the (S) and (C) Xe sites of $XeAr_{12}$ (Figure 18). The agreement between the simulation results for the (C) and (S) sites of $XeAr_{12}$ at $T = 30$ K and the experimentally observed two bands (Figure 18) is reasonable. A more detailed theoretical and experimental analysis of these two bands of $XeAr_{12}$ at $T \geq 30$ K will provide spectroscopic information on the (C) $\rightleftarrows$ (S) dynamic isomerization. What is not understood in the spectrum of $XeAr_{12}$ is the $\delta\nu = 0.66$ eV band (Figure 18), which is also prominent in other small clusters.

(XI.F) Overall Spectroscopic Assignment. The experimental cluster-size dependence of the spectral shifts for distinct Xe site specific absorption bands of $XeAr_N$ clusters, together with our assignments, are presented in Table 7, while Figure 19 portrays the experimental and the calculated cluster size dependence of $\delta\nu$. Here we follow the notation of Möller et al.[58] and label the experimental absorption bands in the order of increasing energy as I′, I, and II for small clusters ($N < 35$) and as I, II, and III for large ($N > 150$) clusters. On the basis of the foregoing analysis for the large cluster size domain the assignment of band III to the (C) site, of band II to interior sites and of band I to the substitutional surface sites seems to be conclusive. We note in passing that the absence of band III in the experimental spectra and in our simulations for $N \leq 120$ (at $T > 15$ K) provides support for the assignment of this band to the high-energy (C) site. The spectral features of site specific excitations in large ($N \geq 130$(calc) and $N \geq 200$(expt)[58−60]) heteroclusters at $T = 30-35$ K are consistent with their general structural characteristics. Moving to the smaller cluster size domain ($N < 35$),[58−60] band I, which is experimentally exhibited at $\delta\nu = 0.23-0.26$ eV, is assigned to the (C) site of the small clusters. This assignment is in accord with the simulated low shifts $\delta\nu = 0.20-0.35$ eV at $T = 30$ K for the (C) site in this small ($N \leq 120$) cluster size domain (section X). On the other extreme of very small clusters ($N = 10-20$), the identification of the (C) site and the (S) sites to bands I and I′, respectively, is reasonable. The low value of $\delta\nu$ calculated for the (C) site of $N = 12$ provides support to its assignment of band I for small ($10 < N < 35$) clusters (Table 7). At present, an assignment of the prominent band II with $\delta\nu = 0.63-0.55$ experimentally observed for $10 < N < 35$[58−60] cannot be provided. The alternative assignment for small clusters, which attributes band I to a surface site and band II to the (C) site, is inconsistent with the results of our calculations for the (C) site energetics in this size domain. We have considered the possibility that the $\delta\nu = 0.63-0.66$ eV band II (for $N < 120$) is not due to $XeAr_N$ but rather to a Xe_2 dimer in a Ar cluster, i.e., Xe_2Ar_N. Preliminary absorption line-shape simulation[122] of the spectra of Xe_2Ar_N clusters ($N = 35-146$) provided spectral shifts in the range $\delta\nu = 0.50-0.60$ eV relative to the bare Xe atom excitation, which is not far in energy from band II. However, careful experimental studies by Möller et al.[58−60] have established that when $XeAr_N$ clusters are synthesized by supersonic expansion of Xe(X) + Ar, the relative abundance of Xe_2Ar_N clusters is negligible for $X \leq 0.01\%$. Only for $X > 0.03\%$ the Xe_2Ar_N ($N \sim 50$) clusters were synthesized with a band at 8.97 eV, i.e., $\delta\nu = 0.53$ eV. This value of $\delta\nu$ is in good agreement with the results of our simulations[122] for Xe_2Ar_N. At present an assignment of the experimental band II for $N = 10-35$ (Table 7) cannot be provided, pointing toward the limitations of the simulations of the cluster structure or of spectroscopic assignments for these small clusters.

XII. Spectral Line Broadening

In the foregoing analysis we have attempted to separate between homogeneous spectral line broadening of a single site and inhomogeneous line broadening originating from the overlap between spectral features of different noncommunicating sites. The calculated single-site homogeneous line widths in the temperature domain 25−35 K are in the range $\Gamma = 0.09-0.15$ eV (Table 6). A heuristic estimate of the dephasing time for the electronic excitation in these clusters is $\tau_D \simeq (c\Gamma)^{-1} = 28-46$ fs (where c is the velocity of light). τ_D is short on the time scale of atomic motion (where characteristic vibration frequen-

TABLE 7: Assignment of the Site-Specific Spectra of $XeAr_N$ Clusters

band index	$\delta\nu$ experiment (eV)[a]	N experiment[a]	assignment	$\delta\nu$ calcd[b] (eV)
I′	0.12	$10 \le N \le 20$	(S) site in very small clusters	0.12
	0.21	$10 \le N \le 20$	(C) site in very small clusters	0.26
I	0.23−0.26	$20 \le N \le 35$	(C) site in small clusters	0.20−0.35
	0.25−0.27	$150 \le N \le 5000$	substitutional surface sites in large clusters	0.15−0.27
II	0.63−0.66	$10 \le N \le 35$	?	
	0.63−0.66	$200 \le N \le 5000$	interior sites in large clusters	0.56−0.42
III	0.77−0.78	$200 \le N \le 5000$	(C) site in large clusters	0.76−0.78

[a] References 58−60. [b] $T = 30$ K for $N = 12$−120 K and $T = 35$ K for $N = 146$, 206.

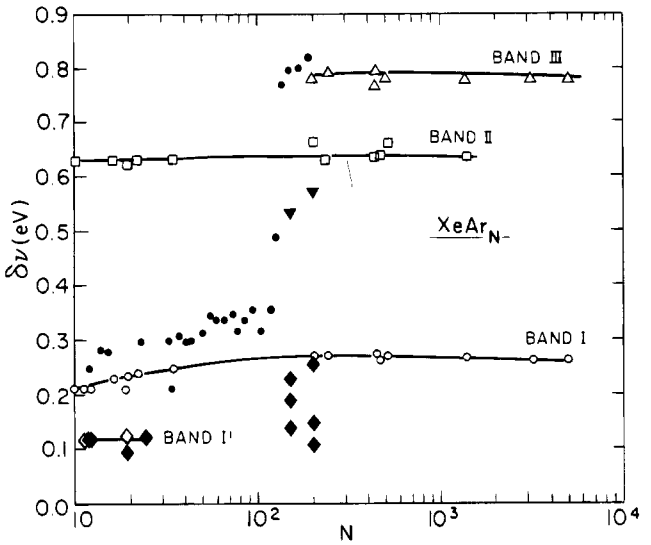

Figure 19. Overview of the experimental and calculated cluster size dependence of $\delta\nu$. Experimental data:[58-60] ◇ band I′ for $N = 10$−20, ○ band I for $N = 10$−35, □ band II for $N = 10$−35 and for $N = 200$−1500, △ band III for $N = 200$−5000. The experimental data points are joined by solid lines to guide the eye. Calculated data: ● (S) Xe substitutional site for small ($N = 12$, 19, 25) clusters at $T = 30$ K and Xe substitutional surface sites for large ($N = 146$, 200) clusters at $T = 30$ K. ▼ Xe interior substitutional site for $N = 146$, 199 clusters at $T = 35$ K. ● Xe central substitutional site for $N = 12$−199 clusters at $T = 30$ K.

cies are ≤50 cm^{-1}) in $XeAr_N$ clusters. Accordingly, in terms of Kubo's line broadening formalism,[105] the electronic excitations of $XeAr_N$ correspond to the slow modulation limit. This conclusion is reinforced by the observation that the line widths (FWHM) obtained from all our simulations are expressed (within an accuracy of 5%) by eq 4.2 in terms of the second central moment of the absorption band, as is appropriate for the slow modulation limit.

It will be instructive to examine the information pertaining to the cluster nuclear dynamics, which emerges from the spectral line broadening. For this purpose we focus on the energy gap correlation function $J(t)$, eq 3.7, and its classical power spectrum $J(\omega)$. The symmetric power spectra, with $J(\omega) = J(-\omega)$, will be decomposed into L individual features, each being characterized by the dispersion Δ_j^2. The power spectra (Figure 20) consist of (1) finite frequency peaks, peaking at frequencies $\{\omega_j\}$; ($j = 2$ to L), which represent intracluster vibrations and (2) a "soft" mode, which corresponds to a zero-frequency peak ($\omega_1 = 0$), manifesting low-frequency slow diffusive motion.

The total dispersion, eq 3.6, is

$$\Delta^2 = J(t{=}0) \int_{-\infty}^{\infty} J(\omega)\, d\omega \qquad (12.1)$$

being given by

$$\Delta^2 = \sum_{j=1}^{L} \Delta_j^2 \qquad (12.2)$$

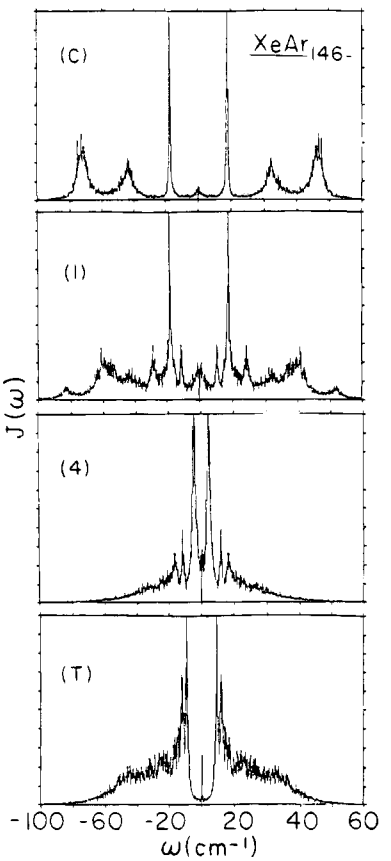

Figure 20. Power spectra for the (C), (1), (4), and (T) Xe substitutional sites in $XeAr_{146}$ at $T = 30$ K.

The power spectra are represented in terms of a superposition of Lorentzians,[73,86,92,93] whereupon the energy gap correlation is represented in terms of a superposition:

$$J(t) = \sum_{j=1}^{L} \Delta_j^2 \cos(\omega_j t) \exp(-\gamma_j |t|) \qquad (12.3)$$

with the frequencies $\{\omega_j\}$, dampings $\{\gamma_j\}$, and dispersions $\{\Delta_j^2\}$. Equation 12.3 constitutes a simplified representation of damped oscillatory motions.[73,86,92,93] The power spectrum of eq 12.3 assumes the form

$$J(\omega) = \frac{2\Delta_1^2\gamma_1}{\omega^2 + \gamma_1^2} + \sum_{j=2}^{L}\left[\frac{\Delta_j^2\gamma_j}{(\omega - \omega_j)^2 + \gamma_j^2} + \frac{\Delta_j^2\gamma_j}{(\omega + \omega_j)^2 + \gamma_j^2}\right] \qquad (12.4)$$

The simulated power spectra were fit by eq 12.4 and a sample of the parameters is presented in Table 8. To assess the

TABLE 8: Parametrization of the Power Spectra $J(\omega)$ of $XeAr_N$ at $T = 30$ K

cluster and site	i	$\omega_j{}^a$ (cm^{-1})	$\gamma_j{}^a$ (cm^{-1})	$\Delta_{(j)}{}^{2a}$ (10^4 cm^{-2})	Δ^b (cm^{-1})	Δ/γ_1, Δ/ω_j ($j \neq 1$)
$XeAr_{12}$	1	0	0.3	0.048		820
(S)	2	14.7	1.6	1.29	246	17
	3	30.9	3.8	1.19		8
	4	52.1	4.9	0.50		5
$XeAr_{54}$	1	0	2.1	3.95		187
(C)	2	21.1	2.2	1.91	393	19
	3	50.5	6.3	1.87		8
$XeAr_{146}$	1	0	1.8	0.57		260
(C)	2	16.0	0.4	2.80	469	29
	3	44.0	3.0	3.11		11
	4	71.7	2.5	4.52		7
$XeAr_{146}$	1	0	2.7	1.38		164
interior (1)	2	9.8	0.4	0.46		45
	3	17.9	1.2	2.43		25
	4	27.7	1.3	1.02	444	16
	5	40.7	3.4	1.44		11
	6	59.0	3.8	2.57		8
	7	81.4	3.3	0.57		5
$XeAr_{199}$	1	0	1.9	0.06		142
surface (8)	2	14.7	1.3	0.98		18
	3	19.5	0.9	0.61		14
	4	22.8	1.7	0.91		12
	5	32.6	1.6	0.22	270	8
	6	39.1	1.5	0.18		7
	7	48.9	3.8	0.53		6
	8	63.5	1.3	0.10		4
	9	74.9	1.8	0.05		4

[a] Parameters from power spectra. [b] $\Delta = [\Sigma\Delta_j{}^2]^{1/2}$.

individual contributions to the line shape, we express the generating function $g(t)$, eq 3.11 in the form

$$g(t) = \sum_{j=1}^{L} g_j(t) \tag{12.5}$$

where for the soft mode

$$g_1(t) = (\Delta_1{}^2/\gamma_1{}^2)[\exp(-\gamma_1 t) - 1 + \gamma_1 t] \tag{12.6a}$$

while for the finite frequency $j \neq 1$ modes

$$g_j(t) = \frac{\Delta_j{}^2}{(\omega_u{}^2 + r_j{}^2)^2}\{(\gamma_j{}^2 - \omega_j{}^2)[\cos(\omega_j t)\exp(-\gamma_j t) - 1 + \gamma_j t] - 2\omega_j\gamma_j \sin(\omega_j t)\exp(-\gamma_j t) + 2\omega_j{}^2\gamma_j t\} \tag{12.6b}$$

The line shape, eq 3.10, is recast (on the energy scale $\omega_{eg} = 0$) in the form

$$L(E) = (1/\pi)\int dt \exp[i(E - \langle U\rangle)t]\prod_j \exp(-g_j) \tag{12.7}$$

We proceed to discuss the individual contributions g_j to the generating function, eq 12.5, assessing the conditions for the applicability of the slow modulation limit. For the soft mode the slow modulation (short-time) limit is realized when the total dispersion $\Delta = [\Sigma_j\Delta_j{}^2]^{1/2}$, determined by eq 12.2, exceeds γ_1, so that

$$\Delta/\gamma_1 \gg 1 \tag{12.8}$$

For the finite frequency components, all the modes correspond to the oscillatory motion, i.e., $\gamma_j \ll \omega_j$. A short time expansion of the generating function (eq 12.6b) is applicable provided that the total dispersion Δ, eq 12.2, is large relative to all the frequencies, i.e.

$$\Delta \gg \omega_j \gg \gamma_j \quad (j \neq 1) \tag{12.9}$$

Equations 12.8 and 12.9 ensure the applicability of the stochastic slow modulation limit. These conditions are well satisfied for the electronic excitation in $XeAr_N$ clusters (Table 8). Accordingly, in the slow modulation stochastic limit, we have $g_j(t) = \Delta_j{}^2t^2/2$ for all the modes j and the total line width being given by $\Gamma = 2.355[\Sigma_j\Delta_j{}^2]^{1/2}$, resulting in eq 4.2. The total line broadening in the slow modulation limit is determined by the superposition of the dispersions of all the modes and being independent of their dampings. This analysis elucidates the interrelationship between spectral line broadening and nuclear dynamics in these elemental clusters.

The exploration of the energetics and nuclear dynamics pertaining to the electronic absorption spectroscopy of elemental clusters provides the basis for the studies of excited states dynamics. Of considerable interest is the dynamics of configurational nuclear relaxation around electronic extravalence excitations.[112] We are currently exploring[122] site-specific nuclear dynamics around Rydberg impurity excitations in $XeAr_N$ clusters. The large configurational dilation, i.e., "bubble formation" around the Rydberg state, will be manifested in a small spectral shift (relative to the free atom for energy) for fluorescence and in a large Stokes shift between emission and absorption. Predictions of the energetics and line shapes of the emission spectra of $XeAr_N$ clusters will provide significant information on the dynamics of large finite systems.

Acknowledgment. We are greatly indebted to Dr. Thomas Möller for extensive prepublication information and for illuminating discussions and correspondence. This research was supported by the Binational German–Israeli Binational James Franck program for laser–matter interaction.

References and Notes

(1) Mackay, A. L. *Acta Crystallogr.* **1962**, *15*, 916.
(2) Hoare, M. R. *Adv. Chem. Phys.* **1969**, *40*, 49.
(3) (a) Hai, V.; Vodar, B. *Z. Elektrochem.* **1960**, *64*, 756. (b) Kudian, A.; Welsh, H. L.; Watanabe, A. *J. Chem. Phys.* **1965**, *43*, 3397. (c) Novick, S. E.; Davies, P.; Harris, S. J.; Klemperer, W. *J. Chem. Phys.* **1973**, *59*, 2273.
(4) Claassen, H. H.; Selig, H.; Malm, J. G. *J. Am. Chem. Soc.* **1962**, *84*, 3593.
(5) (a) Mulliken, R. S. *J. Am. Chem. Soc.* **1950**, *72*, 600. (b) Mulliken, R. S. *J. Am. Chem. Soc.* **1952**, *74*, 811.
(6) (a) Smalley, R. E.; Levy, D. H.; Wharton, L. *J. Chem. Phys.* **1976**, *64*, 3266. (b) Levy, D. H. *Adv. Chem. Phys.* **1981**, *48 (I)*, 323.
(7) Jortner, J. *Ber. Bunsen-Ges. Phys. Chem.* **1984**, *88*, 188.
(8) Bjørnholm, S. *Contemp. Phys.* **1990**, *31*, 309.
(9) *Proceedings of the International Meeting on Small Particles and Inorganic Clusters. J. Phys. (Paris), Colloque C* **1977**, *2*, 38.
(10) *Proceedings of the Second International Meeting on Small Particles and Inorganic Clusters, Lausanne.* 1980. *Surf. Sci.* **1981**, *106*, 1–608.
(11) *Proceedings of Bunsengesellschaft Discussion Meeting on Experiments on Clusters, Koenigstein, 1983; Ber. Bunsen-Ges. Phys. Chem.* **1984**, *88*.
(12) *Proceedings of the Third International Meeting on Small Particles and Inorganic Clusters, Berlin, 1985; Surf. Sci.* **1985**, *165*, 1–1072.
(13) Träger, F., Putlitz, G., zu, Eds. *Metal Clusters. Proceedings of an International Symposium, Heidelberg*; Springer: Berlin, 1986.
(14) Jena, P., Rao, B. K., Khanna, N., Eds. *The Physics and Chemistry of Small Clusters. NATO ASI Series*; Plenum Press: New York, 1986.
(15) Sugano, S., Nishima, Y., Onishi, S., Eds. *Microclusters*; Springer: Berlin, 1987.
(16) Jortner, J., Pullman, A., Pullman, B., Eds. *Large Finite Systems*; Reidel: Dordrecht, 1987.
(17) Benedek, G., Martin, T. P., Pacchioni, G., Eds. *Elemental and Molecular Clusters*; Springer: Berlin, 1988.
(18) Scoles, G., Ed. *The Chemical Physics of Atomic and Molecular Clusters. Proceedings of the International School of Physics "Enrico Fermi", Course CVII*; North Holland: Amsterdam, 1990.
(19) Proceedings of the Fourth International Symposium on Small Particles and Inorganic Clusters, Aix en Provence, 1988; *Z. Phys. D: Atoms, Molecules Clusters* **1989**, *12*.

(20) Echt, O., Recknagel, E., Eds. Proceedings of the Fifth International Symposium on Small Particles and Inorganic Clusters, Konstanz, 1991; *Z. Phys. D: Atoms, Molecules Clusters* **1990**, *19*, 20.
(21) Sugano, S. *Microcluster Physics*; Springer-Verlag: Berlin, 1991.
(22) Berry, R. S., Burdett, J., Castelman, A. W., Eds. Small Particles and Inorganic Clusters; *Z. Phys. D: Atoms, Molecules Clusters* **1993**, *26*, 1.
(23) Jena, P., Khanna, S. N., Rao, B. K., Eds. *Physics and Chemistry of Finite Systems: From Clusters to Crystals*; Kluwer: Dordrecht, 1992.
(24) Jortner, J. *Z. Phys. D* **1992**, *24*, 247.
(25) Farges, J.; De Feraudy, M. F.; Raoult, B.; Torchet, G. *J. Chem. Phys.* **1983**, *78*, 5067.
(26) Farges, J.; De Feraudy, M. F.; Raoult, B.; Torchet, G. *J. Chem. Phys.* **1986**, *84*, 3491.
(27) Echt, O.; Sattler, K.; Recknagel, E. *Phys. Rev. Lett.* **1981**, *47*, 1121.
(28) Echt, O.; Kandler, O.; Leisner, T.; Miehle, W.; Recknagel, E. *Faraday Sym. No. 25, Large Gas Phase Clusters* **1989**.
(29) Martin, T. P.; Näher, U.; Schaber, H.; Zimmermann, U. *Phys. Rev. Lett.* **1993**, *70*, 3079.
(30) Heer, W. de; Knight, W.; Chou, M.; Cohen, M. L. *Solid State Phys.* **1987**, *40*, 93.
(31) Stringari, S. *Phys. Lett. A* **1985**, *107*, 36.
(32) Stringari, S.; Treiner, J. *J. Chem. Phys.* **1987**, *87*, 5021.
(33) Lewart, D. S.; Pandharipande, V. R.; Pieper, S. C. *Phys. Rev. B* **1988**, *37*, 4950.
(34) Even, U.; Amirav, A.; Leutwyler, S.; Ondrechen, M. J.; Berkovitch-Yellin, Z.; Jortner, J. *Faraday Discuss. Chem. Soc.* **1983**, *73*, 153.
(35) Leutwyler, S.; Jortner, J. *J. Phys. Chem.* **1987**, *91*, 5558.
(36) Brumbaugh, D. V.; Kenny, J. E.; Levy, D. H. *J. Chem. Phys.* **1983**, *78*, 3415.
(37) Stephenson, T. A.; Rice, S. A. *J. Chem. Phys.* **1984**, *81*, 1083.
(38) Alfano, J. C.; Martinez, S. J.; Levy, D. H. *J. Chem. Soc., Faraday Trans.* **1990**, *86*, 2503.
(39) Heikal, A.; Banares, L.; Semmes, D. H.; Zewail, A. H. *Chem. Phys.* **1991**, *156*, 231.
(40) Leutwyler, S.; Bösiger, J. *Chem. Rev.* **1990**, *90*, 489.
(41) Amirav, A.; Even, U.; Jortner, J. *Chem. Phys. Lett.* **1979**, *67*, 9.
(42) Amirav, A.; Even, U.; Jortner, J. *J. Chem. Phys.* **1981**, *75*, 2489.
(43) Ben-Horin, N.; Even, U.; Jortner, J. *J. Chem. Phys.* **1992**, *97*, 5988, 6011.
(44) Ben-Horin, N.; Even, U.; Jortner, J.; Leutwyler, S. *J. Chem. Phys.* **1992**, *97*, 5296.
(45) Bahatt, D.; Heidenreich, A.; Ben-Horin, N.; Even, U.; Jortner, J. *J. Chem. Phys.* **1994**, *100*, 6290.
(46) Leutwyler, S.; Bösiger, J. *Z. Phys. Chem. N.F.* **1987**, *154*, 31.
(47) Bösiger, J.; Leutwyler, S. *Phys. Rev. Lett.* **1987**, *59*, 1895.
(48) Bösiger, J.; Leutwyler, S. In *Large Finite Systems*; Jortner, J., Pullman, B., Eds.; Reidel: Dordrecht, 1987; pp 153–164.
(49) Leutwyler, S.; Bösiger, J. *Faraday Discuss. Chem. Soc.* **1988**, *86*, 225.
(50) Bösiger, J.; Knochenmuss, R.; Leutwyler, S. *Phys. Rev. Lett.* **1989**, *62*, 3058.
(51) Knochenmuss, R.; Leutwyler, S. *J. Chem. Phys.* **1990**, *92*, 4686.
(52) Kelley, D. F.; Bernstein, E. R. *J. Phys. Chem.* **1986**, *90*, 5164.
(53) Nimlos, M. R.; Young, M. A.; Bernstein, E. R.; Kelley, D. F. *J. Phys. Chem.* **1989**, *91*, 5268.
(54) Schmidt, M.; Mons, M.; Le Calvé, J. *J. Phys. Chem.* **1992**, *96*, 2402.
(55) Schmidt, M.; Mons, M.; Le Calvé, J. *Chem. Phys. Lett.* **1991**, *177*, 371.
(56) Schmidt, M.; Mons, M.; Le Calvé, J.; Millie, P.; Cossart-Magos, C. *Chem. Phys. Lett.* **1991**, *183*, 69.
(57) (a) Möller, T.; *Z. Phys. D* **1991**, *20*, 1. (b) Wörmer, J.; Möller, T. *Z. Phys. D* **1991**, *20*, 39.
(58) Lengen, M.; Joppien, M.; Müller, R.; Wörmer, J.; Möller, T. *Phys. Rev. Lett.* **1992**, *68*, 2362.
(59) Lengen, M.; Joppien, M.; von Pietorwski, R.; Möller, T. *Chem. Phys. Lett.*, in press.
(60) Möller, T. Private communication and to be published.
(61) Jortner, J.; Koch, E. E.; Schwentner, N. *Electronic Excitations in Condensed Rare Gases*; Springer Tracts in Modern Physics 107; Springer-Verlag: Heidelberg, 1985.
(62) Baldini, G.; Knox, R. S. *Phys. Rev. Lett.* **1963**, *11*, 127.
(63) Baldini, G. *Phys. Rev.* **1965**, *137A*, 508.
(64) Gedanken, A.; Raz, B.; Jortner, J. *J. Chem. Phys.* **1973**, *58*, 1178.
(65) Pudewill, D.; Himpsel, F. J.; Saile, V.; Schwenter, N.; Skibowski, M.; Koch, E. E. *Phys. Status Solidi* **1976**, *74*, 485.
(66) Raz, B.; Jortner, J. *Proc. R. Soc. London, A* **1970**, *317*, 113.
(67) Raz, B.; Jortner, J. *Chem. Phys. Lett.* **1969**, *4*, 511.
(68) Messing, I.; Raz, B.; Jortner, J. *J. Chem. Phys.* **1977**, *66*, 2239.
(69) Messing, I.; Raz, B.; Jortner, J. *J. Chem. Phys.* **1977**, *66*, 4577.
(70) Messing, I.; Raz, B.; Jortner, J. *Chem. Phys.* **1977**, *23*, 23.
(71) Webber, S.; Rice, S. A.; Jortner, J. *J. Chem. Phys.* **1965**, *42*, 1907.
(72) Phillips, J. C. *Solid State Phys.* **1966**, *55*, 18.
(73) Fried, L. E.; Mukamel, S. *Adv. Chem. Phys.* **1993**, *26*, 217.
(74) (a) Gough, T. E.; Mengel, M.; Rowntree, P. S.; Scoles, J. *J. Chem. Phys.* **1985**, *83*, 4958. (b) Levandier, J.; Mengel, M.; Combariza, J.; Scoles, G. *The Chemical Physics of Atomic and Molecular Clusters. Proceedings of the International School of Physics "Enrico Fermi", Course CVII*; North Holland: Amsterdam, 1990; p 331.
(75) Markovich, G.; Giniger, R.; Levin, M.; Cheshnovsky, O. *J. Chem. Phys.* **1991**, *95*, 9416.
(76) Markovich, G.; Giniger, R.; Levin, M.; Cheshnovsky, O. *Z. Phys. D* **1991**, *20*, 69.
(77) Markovich, G.; Pollack, S.; Giniger, R.; Cheshnovsky, O. *Z. Phys. D* **1993**, *26*, 98.
(78) Markovich, G.; Giniger, R.; Cheshnovsky, O. *J. Chem. Phys.*, in press.
(79) Cheng, H. P.; Berry, R. S. *Phys. Rev. A* **1992**, *45*, 7969.
(80) Couchman, P. R.; Ryan, C. L. *Philos. Mag. A* **1978**, *37*, 369.
(81) Kofman, R.; Cheyssac, P.; Garrigos, R. In *Phase Transitions*; Gordon and Breach: Reading, 1990; Vol. 24–26, p 283.
(82) Berry, R. S.; Beck, T. L.; Davis, H. L.; Jellinek, J. *Adv. Chem. Phys.* **1988**, *90*, 75.
(83) Bixon, M.; Jortner, J. *J. Chem. Phys.* **1989**, *91*, 1631.
(84) Reiss, H.; Mirabel, P.; Whetten, R. L. *J. Phys. Chem.* **1988**, *92*, 7241.
(85) Labastie, P.; Whetten, R. L. *Phys. Rev. Lett.* **1990**, *65*, 1567.
(86) Heidenreich, A.; Bahatt, D.; Ben-Horin, N.; Even, U.; Jortner, J. *J. Chem. Phys.* **1994**, *100*, 6300.
(87) Heidenreich, A.; Jortner, J. *Isr. J. Chem.* **1994**, *33*, 467.
(88) Heidenreich, A.; Jortner, J. *Z. Phys. D* **1993**, *26*, 377.
(89) (a) Stillinger, F. H.; Weber, T. A. *Phys. Rev. A* **1982**, *25*, 978. (b) Stillinger, F. H.; Weber, T. A. *Phys. Rev. A* **1983**, *28*, 2408.
(90) Perera, L.; Amar, F. G. *J. Chem. Phys.* **1990**, *93*, 4884.
(91) (a) Kubo, R.; Toyozawa, Y. *Prog. Theor. Phys.* **1995**, *13*, 160. (b) Lax, M. *J. Chem. Phys.* **1952**, *20*, 1752.
(92) Fried, L. E.; Mukamel, S. *Phys. Rev. Lett.* **1991**, *66*, 2340.
(93) Fried, L. E.; Mukamel, S. *J. Chem. Phys.* **1992**, *96*, 116.
(94) Parneix, P.; Amar, F. G.; Bréchignac, Ph. *Z. Phys. D* **1993**, *26*, 217.
(95) Troxler, T.; Leutwyler, S. *Ber. Bunsen-Ges. Phys. Chem.* **1992**, *96*, 1246.
(96) Robertson, G. N.; Yarwood, J. *Chem. Phys.* **1978**, *32*, 267.
(97) Rothschild, W. G.; Soussen-Jacob, J.; Bessière, J.; Vincent-Geisse, J. *Chem. Phys.* **1983**, *79*, 3002.
(98) Thirumalai, D.; Bruskin, E. J.; Berne, B. J. *J. Chem. Phys.* **1985**, *83*, 230.
(99) Mukamel, S. *J. Chem. Phys.* **1982**, *77*, 173.
(100) Mukamel, S. *Phys. Rep.* **1982**, *93*, 1.
(101) Sue, J.; Yan, Y. J.; Mukamel, S. *J. Chem. Phys.* **1986**, *85*, 462.
(102) Islampour, R.; Mukamel, S. *Chem. Phys. Lett* **1984**, *107*, 239.
(103) Islampour, R.; Mukamel, S. *J. Chem. Phys.* **1984**, *80*, 5487.
(104) Ben-Horin, N.; Jortner, J. *J. Chem. Phys.* **1993**, *98*, 9346.
(105) Kubo, R. *Adv. Chem. Phys.* **1969**, *15*, 101.
(106) Klein, M. L., Vanables, J. A., Eds. *Rare Gas Solids*; Academic Press: London, 1976.
(107) Woon, D. E. *J. Chem. Phys.* **1994**, *100*, 2838.
(108) Boyes, S. J. *Chem. Phys. Lett.* **1994**, *221*, 467.
(109) Last, I.; George, T. F. *J. Chem. Phys.* **1993**, *98*, 6406.
(110) Sherwood, A. E.; Prausnitz, J. M. *J. Chem. Phys.* **1964**, *41*, 429.
(111) Stillinger, F. H.; Stillinger, D. K. *J. Chem. Phys.* **1990**, *93*, 6013.
(112) Scharf, D.; Jortner, J.; Landman, U. *J. Chem. Phys.* **1988**, *88*, 4273.
(113) Ophir, Z. *Impurity States in Solid Rare Gases*; M.Sc. Thesis, Tel Aviv University, 1970.
(114) Farges, J.; De Feraudy, M. F.; Raoult, B.; Torchet, G. *Surf. Sci.* **1981**, *106*, 95.
(115) Farges, J.; De Feraudy, M. F.; Raoult, B.; Torchet, G. *J. Phys. (Paris)* **1977**, *38*, C2, 47.
(116) Farges, J. *J. Cryst. Growth* **1975**, *31*, 79.
(117) Klots, C. E. *J. Chem. Phys.* **1985**, *83*, 5854.
(118) Honeycutt, J. D.; Andersen, H. C. *J. Phys. Chem.* **1987**, *91*, 4950.
(119) Wilkinson, P. G. *J. Quant. Spectrosc. Radiat. Transfer* **1966**, *6*, 823.
(120) Beck, T. L.; Doll, J. D.; Freeman, D. L. *J. Chem. Phys.* **1989**, *90*, 5651.
(121) (a) Fraenkel, R.; Haas, Y. *J. Chem. Phys.* **1994**, *100*, 4324. (b) Fraenkel, R.; Haas, Y. *Chem. Phys.*, in press.
(122) Goldberg, A.; Jortner, J., to be published.

JP942600O